

Article

Landslides and Gullies Interact as Sources of Lake Sediments in a Rifting Context: Insights from a Highly Degraded Mountain Environment

Liulsegad Belayneh ^{1,2,*}, Olivier Dewitte ³, Guchie Gulie ⁴, Jean Poesen ^{5,6}, Daniel O'Hara ¹, Alemayehu Kassaye ⁴, Tizita Endale ² and Matthieu Kervyn ¹

- ¹ Department of Geography, Vrije Universiteit Brussel, 1050 Brussels, Belgium; daniel.ohara@vub.be (D.O.); matthieu.kervyn.de.meerendre@vub.be (M.K.)
- ² Department of Natural Resource Management, Arba Minch University, Arba Minch P.O. Box 21, Ethiopia; tizitaendale.elcho@kuleuven.be
- ³ Department of Earth Sciences, Royal Museum for Central Africa, 3080 Tervuren, Belgium; olivier.dewitte@africamuseum.be
- ⁴ Department of Water Resource and Irrigation Engineering, Arba Minch University, Arba Minch P.O. Box 21, Ethiopia; guchie.gulie@amu.edu.et (G.G.); alemayehukasaye.tilahun@kuleuven.be (A.K.)
- ⁵ Department of Earth and Environmental Sciences, KU Leuven, 3000 Leuven, Belgium; jean.poesen@kuleuven.be
- ⁶ Department of Earth Sciences and Spatial Management, Maria Curie-Skłodowska University, 20-718 Lublin, Poland
- * Correspondence: liulsegad.bunare@vub.be



Citation: Belayneh, L.; Dewitte, O.; Gulie, G.; Poesen, J.; O'Hara, D.; Kassaye, A.; Endale, T.; Kervyn, M. Landslides and Gullies Interact as Sources of Lake Sediments in a Rifting Context: Insights from a Highly Degraded Mountain Environment. *Geosciences* **2022**, *12*, 274. <https://doi.org/10.3390/geosciences12070274>

Academic Editors: Jesus Martinez-Frias and Marco Cavalli

Received: 4 May 2022

Accepted: 5 July 2022

Published: 8 July 2022

Publisher's Note: MDPI stays neutral with regard to jurisdictional claims in published maps and institutional affiliations.



Copyright: © 2022 by the authors. Licensee MDPI, Basel, Switzerland. This article is an open access article distributed under the terms and conditions of the Creative Commons Attribution (CC BY) license (<https://creativecommons.org/licenses/by/4.0/>).

Abstract: Like many other lakes in the world, the interconnected Abaya and Chamo lakes in the Southern Main Ethiopian Rift are affected by rapid sediment accumulation. Although land degradation is a well-known issue in this part of the African continent, the main sediment sources, their spatial distribution and interaction in the Abaya–Chamo lakes' basin have not yet been documented. Here, we present a systematic inventory, characterization, and spatial analysis of landslides and gullies as concentrated sediment sources, for four representative river catchments impacted by landscape rejuvenation. Using Google Earth imagery and field surveys, we mapped with high accuracy a total of 7336 gullies and 430 landslides. Recent landslides observed during the last decade were few, small and shallow, and appear to have played a minor role in the current sediment dynamics. Large landslides are old and inactive. Although they do not contribute to the current sediment budget, they contribute indirectly to landscape dynamics by favoring the occurrence of gullies. Overall, large percentages of severe to extremely degraded areas of gully erosion are located in rejuvenated landscapes, especially at the level of the old landslides. Many active gullies are connected to the river network, as such acting as the source of sediment. Our analysis is a step towards understanding the nature and control of anthropic activities on sediment production in the region. We also highlight the importance of considering the interactions between sediment sources and the connectivity of the geomorphological system.

Keywords: gully erosion; landslide; river incision; connectivity; knickpoint; Africa

1. Introduction

Lakes are vital in preserving regional environmental and ecological functions and services [1–3]. However, these functions have been declining, especially in lower-middle-income and low-income countries due to rapid population growth that has accelerated land degradation, increasing sediment delivery to lakes [4,5]. Sedimentation caused by soil erosion significantly reduces the original storage capacity of many lakes. Each year throughout the world, 1–2% of the existing storage volume of reservoirs are lost due to

sedimentation [4]. Despite the problem of sedimentation, many lakes remain unstudied and the role of different land degradation processes in contributing to the sedimentation are often hypothetical.

Excessive sediment load caused by soil erosion in the catchment are one of the main environmental threats that East African lakes are facing [6]. Because of various human-induced impacts, the shallow lakes of the Main Ethiopian Rift are recognized as the most fragile inland waters in Ethiopia [7]. For example, Lake Hawassa in the central Main Ethiopian Rift, has lost 4% of its storage capacity in a decade, due to sedimentation [8].

The catchments of lakes Abaya and Chamo are located in the Southern Main Ethiopian Rift. The area is characterized by severe land degradation resulting in soil erosion in the highlands and sediment accumulation in the lakes [9,10]. The increased sediment deposition rate in Lake Abaya since the 1970s resulted in water level rise and decline in water quality [11]. Preliminary field assessments indicated that concentrated sediment sources, dissecting the land and impacting agricultural production in the catchments of the two lakes, are predominantly gullies and landslides [10,12–14]. However, little information exists for their distribution and influence on Abaya and Chamo.

Gully erosion is a geomorphological process that plays a key role in land degradation by increasing landscape connectivity, transferring runoff and sediments [15,16]. Gullies are highly sensitive to rainfall intensity [17] and land use/land cover (LULC) conditions [18], with gully erosion shown to be a main source of sediment in various environments [16,19,20]. Landslides also act as important erosional processes, providing sediment to rivers in mountainous catchments [19–21]. Landslides are usually triggered by intense or prolonged rainfall and/or seismic activity [22,23]. Shallow landslides (rupture depth less than a couple of meters) are very sensitive to LULC conditions [22,24]. Although the triggering conditions of the two processes are frequently different, landslides and gullies often share similar environmental controls and can often reinforce each other. During development, gullies often cause slope instability processes on their banks [25], or contribute to the reactivation of landslides [26]. Alternatively, landslides change hillslope morphology as well as the hydrological and mechanical properties of the displaced material, often favoring gully formation within the displaced bodies or along their edges [20,27].

The formation and evolution of a tectonic rift is associated with uplift of the rift shoulder and the presence of normal faults and escarpments, e.g., [28,29]. Such tectonic forcing induces a river incision response that is commonly associated with retreating knickpoints, which form the boundary between downstream “rejuvenated” landscapes that are being actively incised, and upstream “relict” landscapes, i.e., terrains with gentler slopes that are not yet affected by the base-level fall and experience little or no river incision. Knickpoint migration upstream rejuvenates the landscape and enforces topographic steepening. These oversteepened hillslopes offer conditions that are commonly more unstable and prone to bedrock landslides [30,31]. Landscape rejuvenation and landslides thus influence regolith availability, impacting gully occurrence [32–37].

The goal of our research is to characterize the importance of gully erosion and landslides as sediment sources, and their potential interactions in the catchments of lakes Abaya and Chamo that have developed in a rifting context. More specifically, a systematic inventory and characterization was conducted for four river catchments on the western border of the Southern Main Ethiopian Rift. Very high spatial resolution satellite information made available by Google Earth imagery was used to conduct a regional-scale inventory that was validated through targeted field surveys. The spatial concentration of these sediment sources was analyzed and interpreted through quantitative comparison with potential controlling factors at a sub-catchment scale.

2. Materials and Methods

2.1. Study Area

Lake Abaya and Lake Chamo are located within the Southern Main Ethiopian Rift (Figure 1). Both lakes are hydrologically interconnected, Lake Abaya flowing towards Lake

Chamo. The brownish color of the waters of Lake Abaya (Figure 1A) is evidence of sediment accumulation [11]. The fact that Lake Chamo seems less disturbed must be nuanced as part of its inflow waters come from Lake Abaya, i.e., waters that have been filtered through the swamps and forested areas that connect the two bodies. Our study focuses on four river catchments of similar size (~200–230 km²), the Shafe and Basso draining to Lake Abaya, and the Sile and Elgo draining to Lake Chamo. This study excludes the flatter alluvial fans, the lacustrine deposits and the central depression of the Elgo catchment (Figure 1). Those catchments were selected as being representative of the small and steep catchments draining the western shoulder of the rift, displaying large gradients in elevation, lithology, LULC and tectonic influence as well as various levels of land degradation. The topography of the studied catchments is characterized by plateaus to the west, transitioning into an eastward-dipping slope marked by sharp topographic escarpments (Figure 1). Indeed, the terrain is characterized by a series of parallel normal faults creating sharp changes in slope across the catchments [28,38]. Similarly to what has been shown by [39] in the Central Main Ethiopian Rift, we assume that these faults are the origin of knickpoints that contribute to the formation of river disequilibrium. With an elevation difference >2500 m, the influence of topography on local climate, soil, vegetation, and settlement patterns is evident in the catchments from the rift floor to the highlands [40].

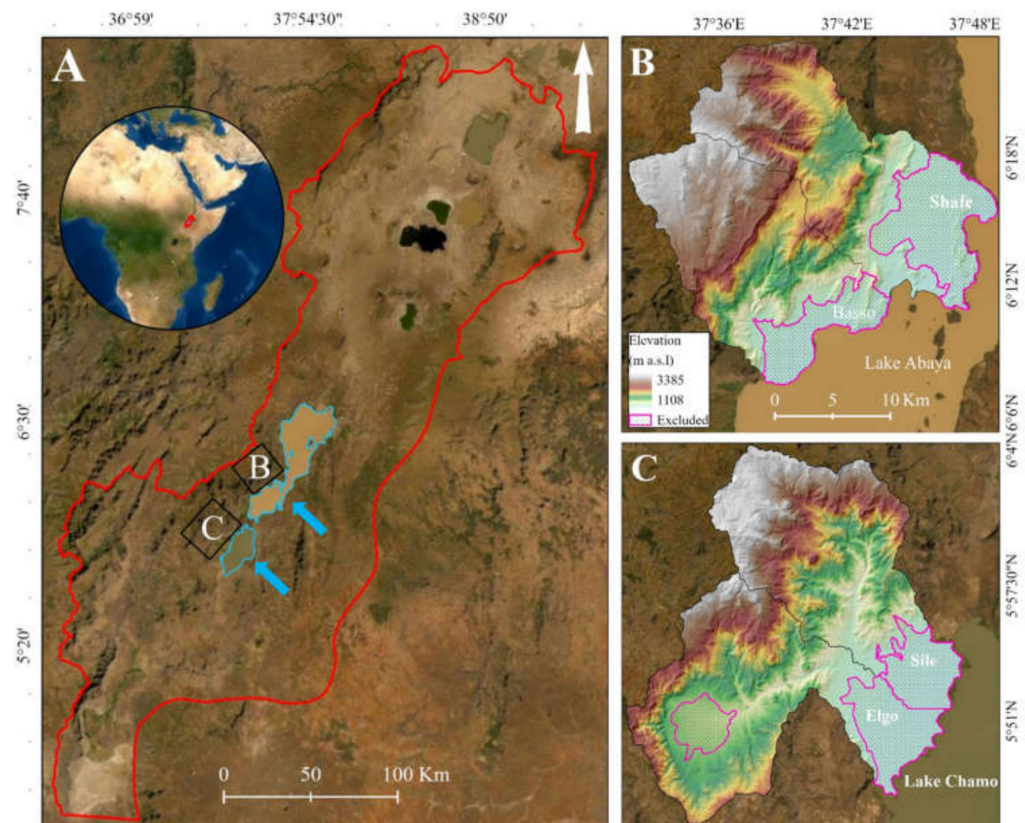


Figure 1. Location of the study area. (A) Lakes Abaya and Chamo within the Main Ethiopian Rift (blue arrows). The contrasting sediment patterns between the two lakes can also be visualized. The red line delineates the lakes' basin. (B) Shafe and Basso, draining to Lake Abaya, and (C) Sile and Elgo, draining to Lake Chamo. Pink polygons with the dots represent the flatter areas excluded from the analysis. Background imagery is from Google Earth (15 June 2020).

The Abaya–Chamo lakes' basin, as part of the Main Ethiopian Rift, was formed by graben subsidence associated with tectonic extension and volcanic activity since the Miocene [28,38]. The geology of the study area is dominated by intrusive and extrusive igneous rocks, including basalts and trachyte lava flows (BTL), as well as lava flows and ignimbrite of trachytic to rhyolitic composition (ITR). Extended Holocene fluvial (fans) and

lacustrine deposits cover the bottom of the rift valley [9]. Unconsolidated sedimentary material are also found along rivers. The major soil types identified in the area are Vertisols, Nitisols, Fluvisols, and Cambisols [41]. Nitisols and Cambisols are the dominant soil types [42].

The catchments are characterized by a tropical savanna climate [43] with two wet seasons end of March to mid-June, and mid-September to late November [44]. Meteorological conditions are highly dependent on elevation in the area, influenced by a combination of synoptic and local circulations that lead to high variability in the temperature, clouds, and precipitation patterns [40,45]. The average annual rainfall varies from ~800 mm in the lowlands to ~1000 mm in the highlands [46]. The main LULC types identified in the area are agricultural land, bare land, rangeland and forest land. LULC map of the year 2019 shows that, agriculture, being the main income-generating activity, dominates the landscape (i.e., 31%).

2.2. Data and Methods

Gully and landslide inventory maps are required to investigate the distribution of these sediment sources and the landscape characteristics associated with their occurrence. Different mapping methods, from field work to satellite images, can be used to create gully and landslide inventory maps [47–50]. Here, we used Google Earth imagery [24,51], which provides very-high (<1 m) spatial resolution images for our study area. We used satellite images acquired mainly in 2016–2019. Geomorphological field mapping was used extensively for validation.

The contribution of gullies to the sediment budget depends on their activity status, which determines how quickly their geometry evolves, the amount of sediment produced and delivered downstream and their associated impacts [52]. Gully activity was constrained from Google Earth imagery as active, partially active and inactive [52,53]. A gully is considered as active if it shows signs of active erosion, i.e., bare gully walls and bed, and/or fresh sediments deposited in the lower parts of the gully. An inactive gully is covered by dense vegetation and assumed not to produce much sediment currently. Partially active gully is an intermediate between active and inactive gully. Similarly, landslides are classified as active [54,55] when they present disturbed vegetation patterns and bare soil surfaces on an image. For the deep-seated landslides, the presence of fresh and sharply defined features such as steep headwall and flanks, and hummocky slopes are also indicators of active mass movements, independent of the vegetation disturbance. Inactive and old landslides are either fully vegetated or they can be partly (or heavily) dismantled by erosion. Finally, connection of the gullies and landslides to the river system is also an essential factor controlling the delivery of sediment to the lowlands [21,56]. A gully and/or landslide is considered to be connected to a river if its lower part is directly along a riverbed, and not connected if the sediments are deposited in fans away from the river network.

Remote sensing inventories need to be validated through ground truthing [48]. The mapped gullies and landslides were thus verified using handheld GPS along transects, over three months in 2018 and 2019. Transects were conducted in 30% of the sub-catchments over a total length of 308 km.

The gully and landslide inventories were then analyzed to understand factors controlling their occurrence and spatial distribution. Most of the gully analyses were conducted at sub-catchment scale, i.e., catchment of the first-order streams. The sub-catchments are hydrological regions, between drainage and divide lines. They were automatically derived from 1 arcsec (30 m) resolution Shuttle Radar Topography Mission digital elevation model (SRTM DEM) based on flow accumulation thresholds and minimum surface area [57,58]. A total of 277 sub-catchments ranging from one to 17 km² were delineated, dividing the four catchments into 55–81 geomorphological units. Gully length density (abbreviated as GLD), in km of gully length per km², was computed for each subcatchment, excluding sub-catchments with no gullies. Using previous GLD classifications [59–61], we denote areas having GLD >5 km km⁻² as extremely degraded, 2.5–5 (very severely degraded),

1–2.5 (severely degraded), 0.5–1 (moderately to severely degraded), 0.1–0.5 (moderately degraded), and $<0.1 \text{ km km}^{-2}$ as not degraded. The influence of potential controlling factors on the occurrence of gullies was analyzed by considering their spatial variation relative to the GLD at sub-catchment scale. The potential controlling factors considered for landslides and gullies are associated with:

- The nature of the topography: knickpoints and landscape rejuvenation, elevation, slope angle, distance to river, and the presence of landslides;
- The nature of the lithology and the regolith: obtaining information on the spatial distribution of the regolith, its nature and its depth can be challenging [35,62,63]. Here, we used information on the lithology and soil properties as proxy, together with the relative age of the topography inferred from presence of landscape rejuvenation.
- The anthropogenic factors: LULC and its dynamics, population density, and road density.

To identify the locations of knickpoints, we utilized TopoToolbox's automatized algorithm [64] on SRTM DEM of the catchments from USGS Earth Explorer data, assuming a 1 km^2 drainage area threshold for channel initiation. Following [24], we distinguish knickpoints from background topographic variation using the maximum difference between the 10th and 90th percentile of relief in smoothed river profiles within each subcatchment. These knickpoints were used to separate the rejuvenated (i.e., zones situated at elevation between the main faults and the knickpoints that propagated upward from it) and relict (i.e., zones above the knickpoint or downward from the main faults) landscapes [24]. The SRTM data was also used for the extraction of elevation and slope angle. The lithologies of Shafe and Basso were digitized from the 1:250,000 geological map produced by the Geological Survey of Ethiopia [65], whereas lithology of Sile and Elgo were mapped using fieldwork. Soil texture was extracted from the Africa Soil Information Service (AfrSIS) soil grids database with 250 m spatial resolution [66]. LULC maps for the four river catchments were produced using supervised spectral classification for the years 1986, 2003 and 2019 using data from Landsat 5, 7 and 8, respectively. Overall, the LULC classification accuracy (~90%) and kappa (~0.87) statistics showed excellent agreement between remote sensing imagery and the ground reference data [67]. Population data for the year 2020 from the 93 kebeles (the most local administrative level) that cover the study catchments were used to compute population density for each sub-catchment. Population density ($\# \text{ km}^{-2}$) of each sub-catchment was computed by estimating the sub-catchment population based on an area-weighted sum of the population contribution of the different kebeles covering the sub-catchment, assuming homogeneous distribution of population, and dividing by total area (km^2) of the sub-catchment. The road network was mapped using Google Earth imagery and field experience, and then road length density computed. The gully number density within and outside the landslides were compared to infer on the interaction between landslides and gullies. As such, the presence of landslides was used as a potential controlling factor of the distribution of the gullies. This analysis was not carried out at a sub-catchment scale.

3. Results

3.1. Inventory, Spatial Distribution and Characteristics of Gullies

Ground control points were collected for 538 gullies using GPS. Gullies identified in the field showed no major deviation from the Google Earth inventory, with an accuracy of 96%. The few false negative and false positive were attributed to gullies of very limited size ($\leq 1 \text{ m}$ wide), with dense vegetation cover, and/or limited contrast between the gullies and the surrounding surface on some images available in Google Earth. In total, the inventory built from Google Earth imagery across the four studied catchments contains 7336 gullies (Figure 2). The gullies are distributed across 215 of the 277 sub-catchments. Gullies are mainly found in the upper and central parts of the Shafe, in the midlands of the Sile and scattered around the central Dembele depression in the Elgo catchment. About 50% of all mapped gullies were identified in Shafe where they are highly concentrated (Table 1). In contrast, gullies are much less frequent in the neighboring Basso, except for one deeply

incised sub-catchment in its northern border. Gullies are totally absent from the flatter lowlands and the central depression of the Elgo, (i.e., areas of mean slope angle $<5^\circ$).

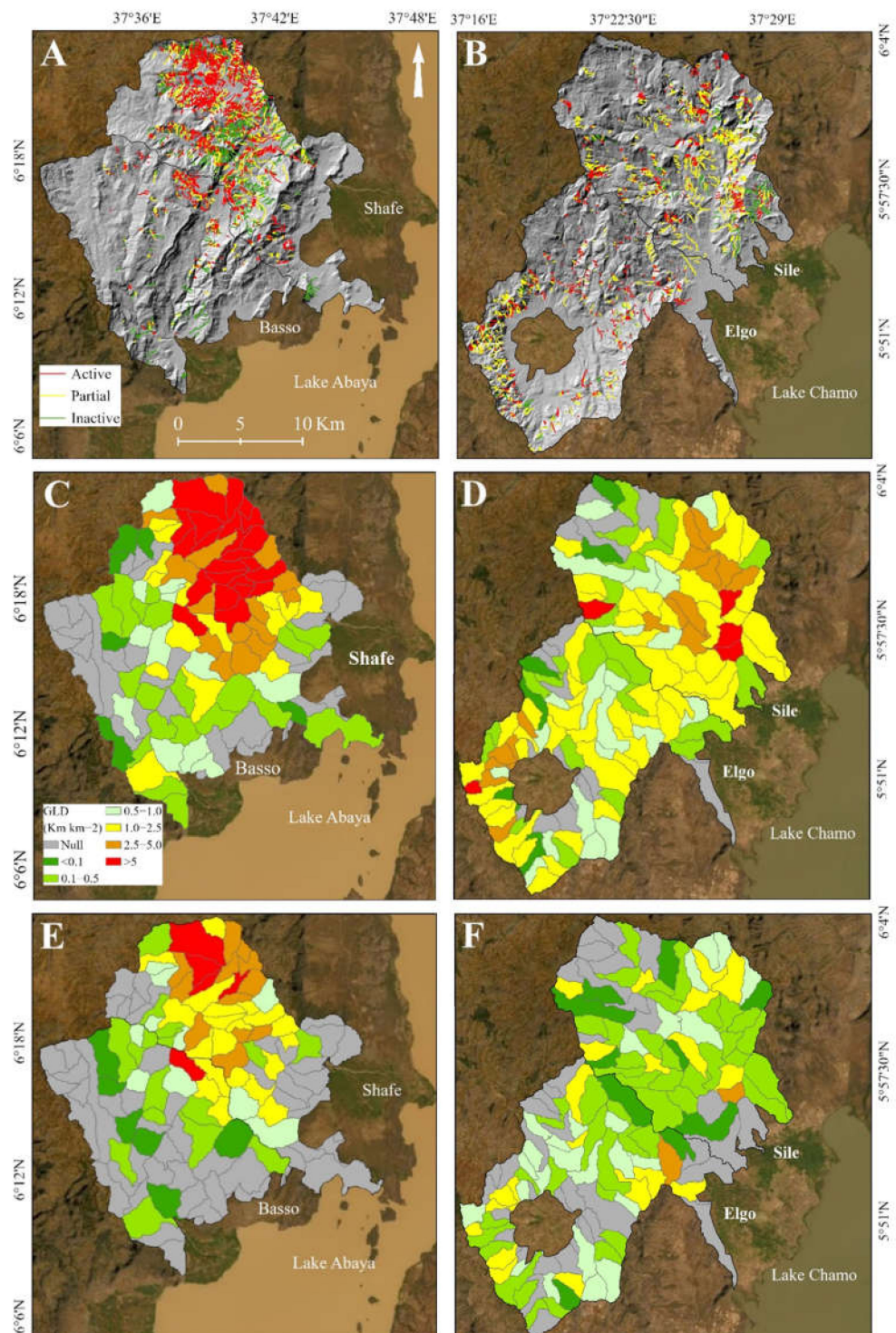


Figure 2. Gully inventory (A,B) and the corresponding GLD for all (C,D) and only active (E,F) gullies. The densities are represented at the level of the sub-catchments. The hillshade in (A,B) is from the 30 m SRTM DEM [68]. Background imagery is from Google Earth (15 June 2020).

Table 1. Summary of the characteristics of gullies per river catchment.

Gully Characteristics	Shafe	Basso	Sile	Elgo	
Total area of the catchment (km ²)	205	209	231	226	
Total number of gullies (#)	3640	823	1748	1125	
Total gully length (km)	716	121	366	228	
Maximum gully length (km)	2.4	2.1	2.1	2.0	
Mean gully length (km)	0.2	0.1	0.2	0.2	
GLD for all gullies (km km ⁻²)	3.5	0.6	1.6	1.0	
Gully status (%)	Active	63	65	38	53
	Partially active	14	23	53	28
	Inactive	23	12	9	19
Gullies connected to a road (%)	9	6	18	25	
Gullies active and connected to road (%)	4.4	3.3	7.9	13.2	
Gullies active and connected to river (%)	15	29	21	26	

Of all the gullies mapped in the study area, 56% are considered as active, this proportion being larger in the Basso (>60%, Table 1), than in the other three catchments. Of the active gullies, 20% are directly connected to the river system. Connections of the gullies to the river network are more common in the Sile (Table 1, Appendix A Figure A1).

High contrasts in GLD are observed across the sub-catchments (Figure 2): the highest GLD computed in the highland sub-catchments of Shafe for all gullies (10.6 km km⁻²) is 1.6 times higher than the highest GLD values recorded for Sile sub-catchments. The GLD of the study area is 1.6 km km⁻², indicating that a significant proportion of the area is severely degraded. According to the GLD classification [59–61], 54% of our study area can be categorized as severely to extremely degraded, 41% as moderately and moderately to severely degraded, and only 5% has a low degradation level.

Even when considering only active gullies, 29% of the study area is still characterized by severe to extreme degradation and 57% by moderate and moderate to severe degradation, highlighting that gully erosion is currently a significant and widespread erosion process in the study area. With its higher fraction of active gullies, the Shafe catchment (i.e., 53% of the area classified as severely to extremely degraded considering only active gullies) stands out even more, relative to the three other catchments, when considering only active gullies. As the average length of gullies is similar between catchments, a similar spatial contrast is obtained when considering the number of gullies per km² instead of their length. The average number of gullies per km² in the area is 10.

3.2. Inventory, Spatial Distribution and Characteristics of Landslides

Ground validation was conducted for 99 landslides. The landslides identified in the field showed no major deviation from Google Earth imagery, with an accuracy of about 90% (2% false positive and 8% false negative). The completeness of the Google Earth inventory was affected by small and shallow landslides noticed in the field, but not identified on the images, as well as other features that were miscataloged as landslides, based on images. In total, the inventory built from Google Earth imagery across the four catchments contained 430 both active and inactive landslides (Figure 3). The landslides cover 131 km² (~15%) of the study area. Active landslides (44%) are commonly small and shallow active processes; reactivation of large landslides being only a few. The active landslides represent 1.3% of the total area affected by slope instabilities, highlighting the contrast in size with the large inactive landslides (Table 2).

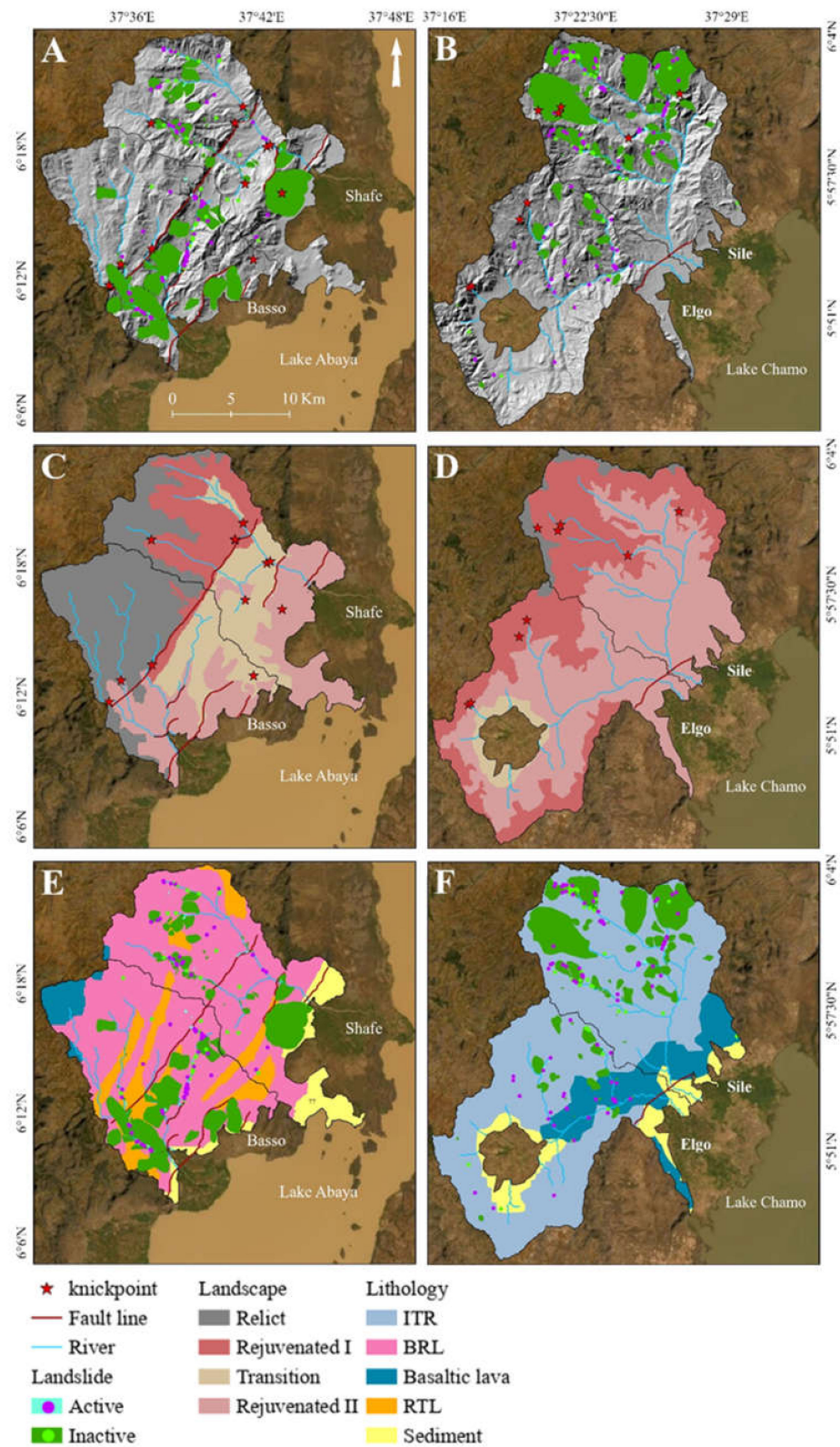


Figure 3. Landslide inventory classified by the level of activity (A,B), landscape rejuvenation (C,D), and lithology (E,F). Landslides $<0.014 \text{ km}^2$ are represented as dots for visibility on maps. In Shafe and Basso, $>70\%$ of the area is basaltic and rhyolitic lava flows (BRL), and $\sim 10\%$ is rhyolites and trachytic lava (RTL). In Sile and Elgo, more than two thirds of the area is dominated by ignimbrite of trachytic to rhyolitic (ITR) composition. The hillshade is from the 30 m SRTM DEM [68]. Background imagery is from Google Earth (15 June 2020).

Table 2. Summary of the characteristics of landslides per river catchment.

Landslide Characteristics	Shafe	Basso	Sile	Elgo	
Total number of landslides (#)	104	107	148	71	
Total area covered by landslides (km ²)	29	38	56	8	
Total area covered by the active landslides (km ²)	0.4	0.6	0.5	0.2	
Area of the largest landslide (km ²)	12.2	5.2	15.5	1.2	
Mean area of the landslides (km ²)	0.3	0.4	0.4	0.1	
The ratio of shallow/deep-seated landslides	36/68	35/72	54/94	29/42	
Landslide (all)-point density in rejuvenated and relict landscapes, respectively (# km ²)	0.7, N	1.1, 0.2	0.7, N	0.4, N	
Active landslide-point density in rejuvenated and relict landscapes, respectively (# km ²)	0.2, N	0.6, 0.1	0.3, N	0.2, N	
Landslide-area density (km ² km ⁻²)	0.2	0.3	0.3	0.0	
Activity of landslides (%)	Active	32	53	45	46
	Inactive	68	47	55	54
Landslides connected to the river (%)	90	94	93	70	
Landslides active and connected to the river (%)	32	52	50	32	

NB. N represent the absence of landslide in relict landscape.

Inactive landslides are commonly larger and older, their age being undetermined. These landslides are partially or fully covered by vegetation and are, to some extent, reworked by human activity. The largest landslides (>0.1 km²) clearly have a long-term morphologic legacy on the landscape, and are located in the midlands of the Shafe and Basso, as well as the upper part of Sile. These are deep-seated landslides, with some earthflows also being present. About 50% of the active landslides are developed within older inactive landslides. Of the total landslides mapped, 89% have their toe in direct contact to the rivers (out of the connected landslides, 45% are active), showing the potential capacity of landslides to directly deliver sediment to the hydrological network.

Active landslides are commonly observed along gully banks (Figure 4). These slope instabilities are usually very small and are difficult to distinguish from the images in Google Earth; larger landslides are much less frequent (Figure 4A,B). Gully erosion is commonly present in large landslides (Figure 4C,D, Table 3, see Section 3.3.4 for further details).

The spatial distribution of knickpoints along the channels is illustrated in Figure 3C,D. Several of these knickpoints were confirmed during field work through the presence of waterfalls or steep river stretches. Shafe, Basso and Elgo are characterized by four landscape zones with three levels of knickpoints: a relict landscape upstream from the highest knickpoints, rejuvenated phase I, rejuvenated phase II and a transition zone between phase I and phase II. The Sile catchment is characterized by relict, rejuvenated phase I and rejuvenated phase II landscapes, the latter occupying the largest area.

The spatial connection between catchment slopes, mapped faults, and the river profiles suggests that many of these knickpoints likely originate from faults (Figure 5) as already highlighted in the Central Main Ethiopian Rift [39]. In the Shafe (Figure 5A), two sets of knickpoints at ~1700 and 1900 m elevations are likely associated with ruptures of the faults downstream of each cluster. Furthermore, a single knickpoint in the upper reach of the Shafe defines the boundary between the relict and rejuvenated landscape with higher mean slopes and more landslides downstream of the knickpoint. This knickpoint occurs within the southern branch of the upper Shafe, but we note that an associated knickpoint is missing from the northern branch, where the boundary between the relict and rejuvenated landscape is further upslope from the channel network, suggesting this transient signal has already propagated through the northern catchment. Within the mid and upper reaches

of the Basso (Figure 5B), a clearly defined cluster of knickpoints at ~2400 m elevation is likely related to mapped faults downstream, also suggesting recent fault activity. Such associations are less evident for the Sile and Elgo catchments (Figure 5C,D). This, in part, is due to the lack of topographic signatures for faulting within this area, as well as a lack of correlation between knickpoints and regional slope angle distributions. Despite this, some knickpoints are distinguishable from the river profiles. Within the Sile, a group of knickpoints that span two branches of the river network at ~2000 m elevation do not coincide with slope angle increases. Similar sets of knickpoints in the Elgo at ~1800 m and 2200 m elevation show no relationship with slope angle, and suggest less tectonic activity and/or at the incipient stage of rifting compared to the Basso and Shafe [39]. This interpretation is also supported by the more dendritic topology and amount of channel branching within the Sile and Elgo catchments compared to Shafe and Basso.

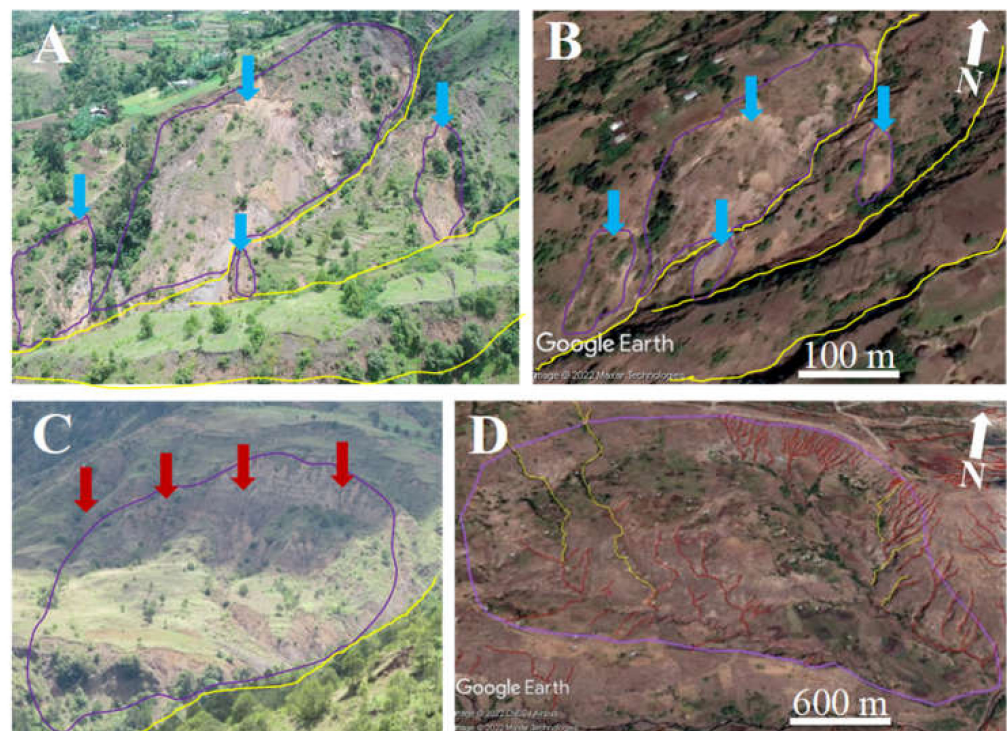


Figure 4. Examples of landslide-gully interactions from Shafe. (A) Field observation of active landslides developed from a gully bank (18 September 2021). (B) Landslides along gully bank (same place as (A)) mapped from Google Earth imagery (6°19'2.27'' N, 37°38'22.32'' E). (C) Field observation of inactive landslide (5 May 2018). The red arrows represent the heads of major active and partially active gullies within the landslide. (D) Active and partially active gullies developed in a large old inactive landslide mapped from Google Earth imagery (6°21'30.64'' N, 37°38'41.52'' E). Gullies connected to the rivers can be observed (C,D). Most of these gullies are active, they can transport significant amount of soil to the lowlands during intense rainfalls. Landslide head scarps (blue arrows); active gullies (in red); partially active gullies (in yellow); landslides (in violet).

Table 3. Landslide and gully interaction for each landscape of the river catchments.

		Shafe	Basso	Sile	Elgo						
Total # of Gullies (All) within Landslides		501	205	499	56						
Total # of Active Gullies within Landslides		367	137	256	32						
GD _{in} : GD _{out} and GLD _{in} : GLD _{out} landslide	Landscape	Gully activity		GD	GLD	GD	GLD	GD	GLD	GD	GLD
	Rejuvenated I	All		33:46	5:8	6:25	1:3	3:6	<1:1	3:4	<1:1
	Rejuvenated II	All		2:7	<1:1	2:3	<1:1	21:9	3:2	8:7	1:1
	Transition	All		26:13	3:3	14:6	1:1	N	N	N	N
	Relict	All		N	N	6:4	1:<1	17:3	2:1	N	N
	Rejuvenated I	Active		28:28	3:4	97:13	8:1	2:2	<1:<1	3:1	<1:<1
		Inactive		6:9	1:2	N:1	N:<1	2:<1	<1:<1	N:<1	N:<1
	Rejuvenated II	Active		34:3	3:<1	6:<1	<1:<1	13:3	1:<1	11:3	1:<1
		Inactive		1:2	<1:1	2:1	1:<10	3:1	<1:<1	5:<1	1:<1
	Rejuvenated I and II	Active		29:16	3:2	7:2	1:<1	5:3	1:<1	9:2	1:<1
Inactive			3:6	<1:1	2:1	1:<1	2:1	<1:<1	5:<1	1:<1	

GD_{in} and GD_{out} are gully number density inside and outside the landslides (# km⁻²), whereas GLD_{in} and GLD_{out} are gully length density inside and outside the landslides, respectively. All gullies include active, partially active and inactive gullies. N either means the landscape does not exist in the catchment and/or landslides do not host gullies in that landscape.

Most of large deep-seated landslides are located downslope of the knickpoints in the rejuvenated landscapes. Within two rejuvenated landscapes, 21% of the hillslope areas are affected by landslides. In the Shafe, a spatial relationship is noticed—a series of landslides occur downstream of the western-most knickpoint, while the sub-catchment to the north has the largest amount of small active and inactive landslides towards the top of the rejuvenated zone. The lithological control on the landslides is less evident to demonstrate here since most of the rejuvenated landscapes are characterized by one dominant group of rock types, namely BRL for the Shafe and Basso catchments and ITR composition for the Sile and Elgo catchments (Figure 3).

3.3. Controlling Factors of Gully Erosion

The potential factors controlling the spatial variation in GLD were tested for the whole gully inventory, and for active and inactive gullies separately. For facilitating the comparison between catchments, the GLD value of each sub-catchment was standardized by considering the deviation relative to the average of each catchment [69]. A negative GLD value indicates a value less than the average of each catchment, whereas a positive value indicates the opposite. This analysis was limited to sub-catchments with observed gullies.

3.3.1. Topographic Controls

We observed a non-linear relationship between GLD, elevation and mean slope angle of each sub-catchment (Figure 6). GLD was highest for elevation between 1700–2600 m and for slope angle between 10–20° in the Shafe, while no clear association was observed in the Basso. In the Sile, the density was highest at an elevation of 1400–1600 m, with one exception of a catchment at 2500 m, and no clear association with mean slope angle was observed. For the Elgo, the highest GLD was concentrated at an elevation of 1400–1900 m and for a slope angle between 15–35°.

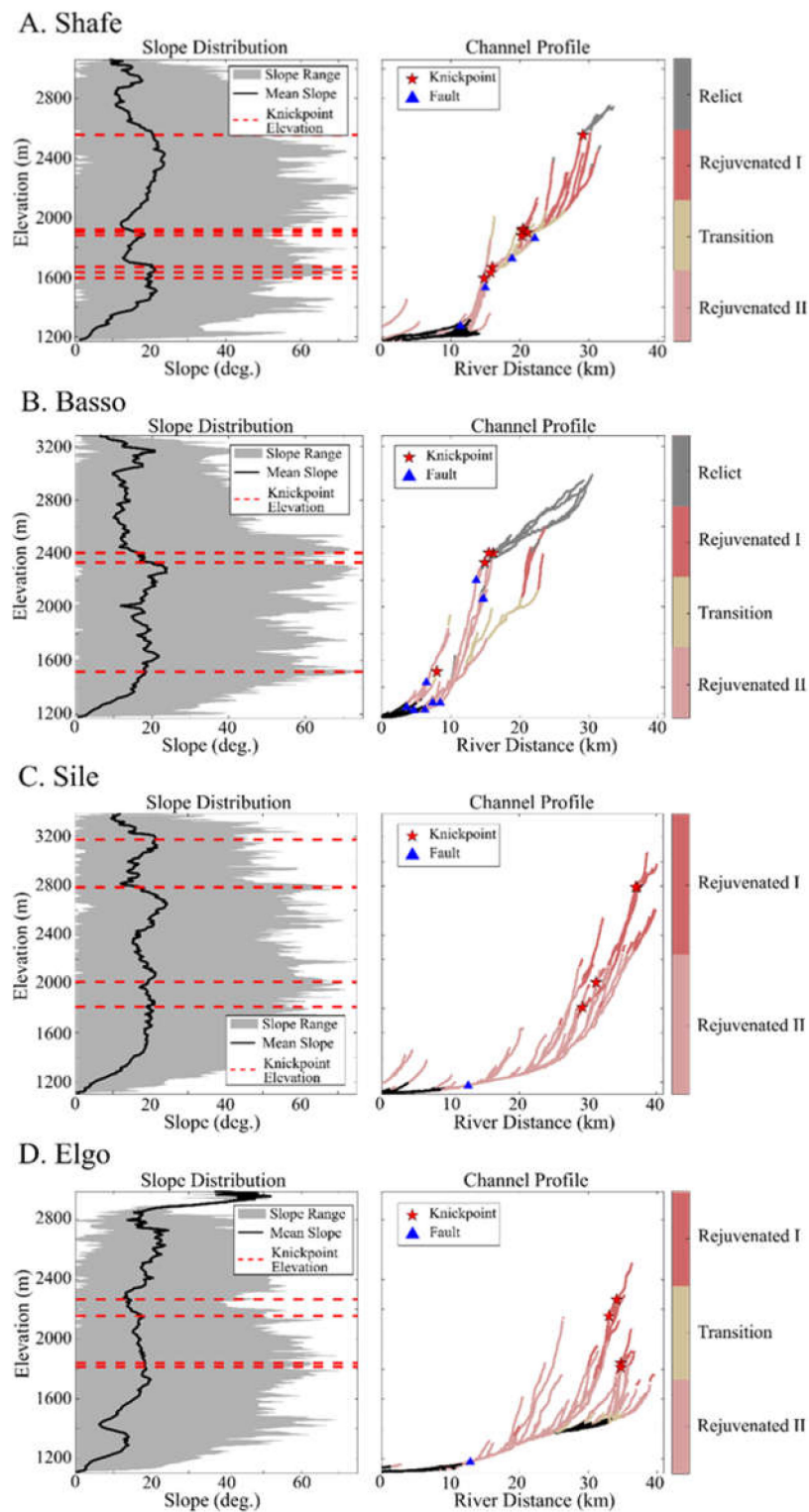


Figure 5. Relationship between slope angle (left) distributions with knickpoints, mapped fault intersections, and landscape rejuvenation alongside river profiles (right) for the (A) Shafe, (B) Basso, (C) Sile, and (D) Elgo catchments. Gray shading and black lines (left plots) are the range and mean catchment slopes at each elevation, respectively; red-dashed lines are the elevations of knickpoints. Lines (right plots) are river profiles as a function of upstream distance, colored by landscape classification.

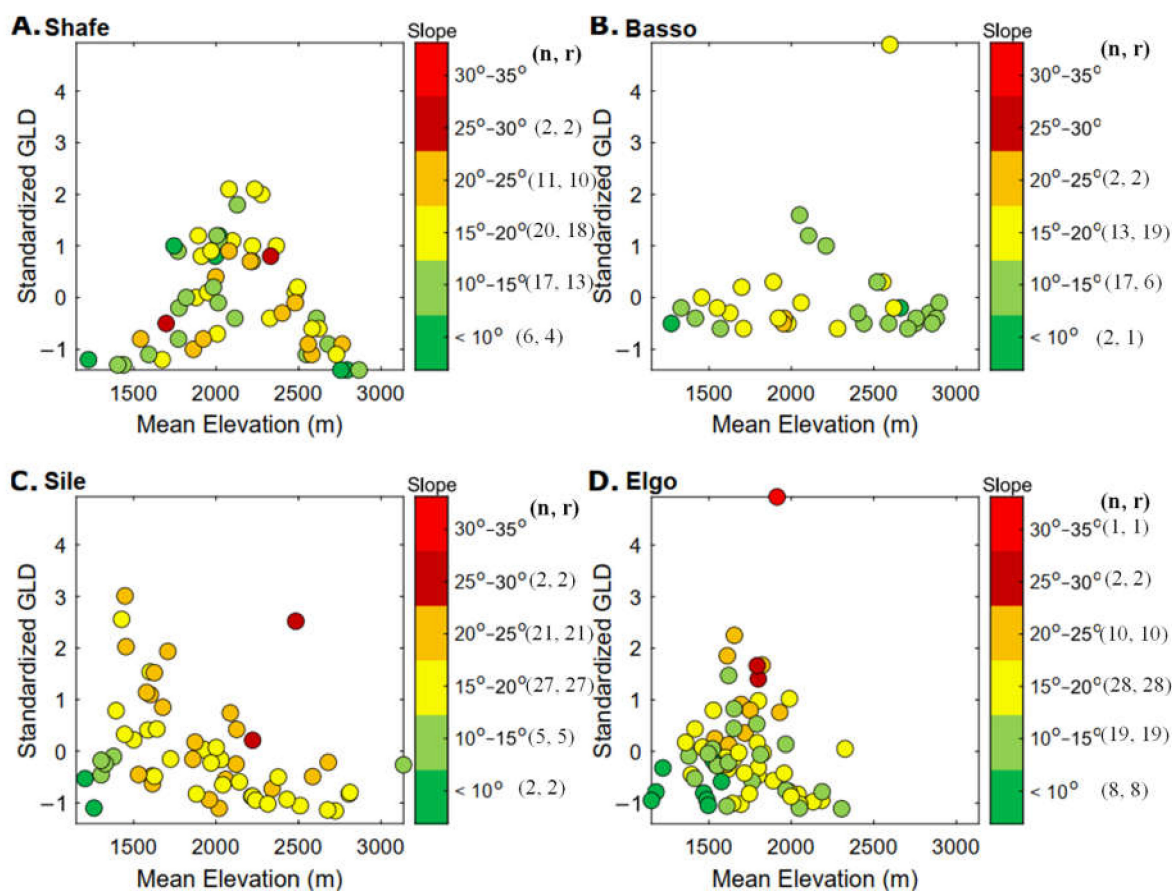


Figure 6. Relationships between GLD, mean elevation and mean slope angle for each sub-catchment of the four study catchments. Symbols are colored based on slope angle. n represents number of sub-catchments of the stated slope angle category in degrees, and r represents number of sub-catchments of each slope angle category in the rejuvenated landscape. In Sile and Elgo, only sub-catchments in rejuvenated landscape are affected by gully features.

In all catchments, the highest GLD and percentage of severely to extremely degraded areas were in the rejuvenated landscapes (i.e., rejuvenated phase I, II and transitional), showing a positive relationship between these landscapes and GLD (Figures 3 and 7). In the Shafe, high GLDs were dominant in the rejuvenated phase I, whereas the rejuvenated landscape II was characterized by higher GLD in the Sile and Elgo. Note that in Basso, the highest GLD was observed in relict landscape at the level of one sub-catchment.

3.3.2. Lithologic and Soil Controls

In the Shafe, a large range in the GLD was noted for the most common lithology of basalt and rhyolitic lava (BRL) (Figure 8). Rhyolite and trachytic lava (RTL) is associated with the highest GLD median. Although the GLD values are generally lower for the Basso, we observed a broader range with some high density values for BRL lithology, including two outlier sub-catchments. In the Sile and Elgo, there was little contrast in the range of GLD among the different lithologies, although higher values were reached in ITR, the dominant lithology in the rejuvenated landscapes.

The clay ratio of soil, calculated as the percentage of sand and silt fractions over the percentage of clay, is used as an index of soil erodibility [70], with low clay-ratio soils considered to have a low erodibility and higher-ratio soils to be more erodible [70]. Except in the Sile, where the clay ratio is increasing as the GLDs decrease, no clear relation between clay ratio and density was observed in the other three catchments (Appendix A Figure A3).

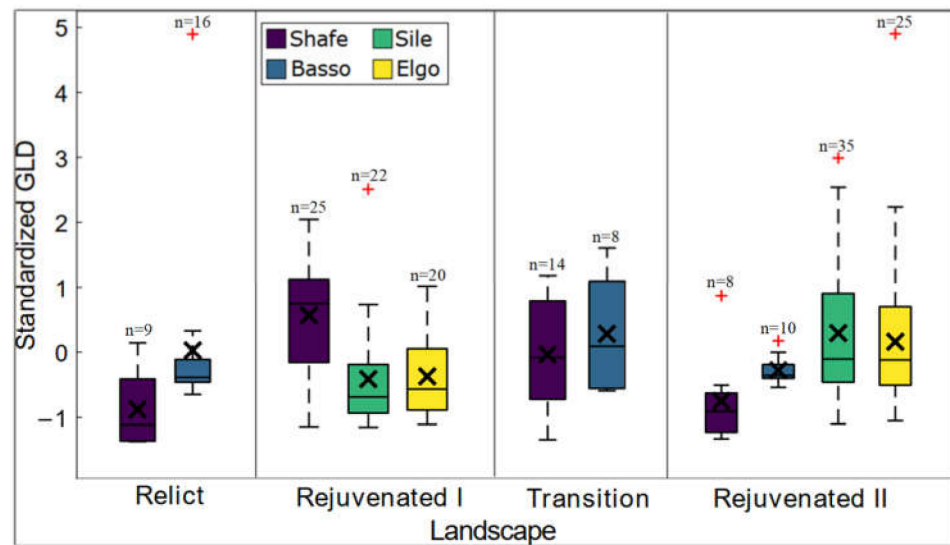


Figure 7. Boxplot of GLD for the different landscape zonation based on knickpoint locations for each sub-catchment of the four study catchments. Boxplots give lower and upper quartiles and median. The mean GLD represented by X. Outliers beyond whiskers are shown as +. The n values above each boxplot indicate the number of sub-catchments.

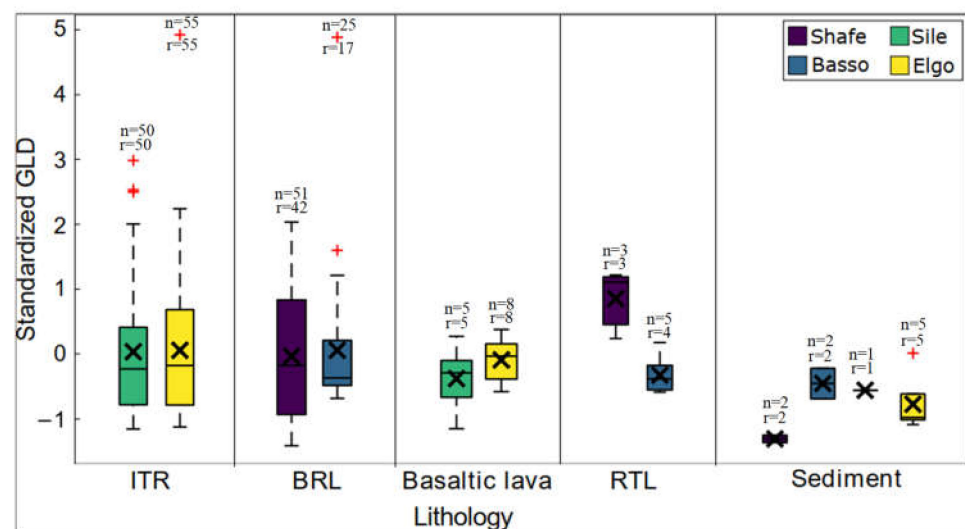


Figure 8. Relationships between lithology and standardized GLD per river catchment. Boxplots give lower and upper quartiles and median. The mean GLD represented by X. Outliers beyond whiskers are shown as +. n represents the number of sub-catchments for each type of lithology and r represents the number of sub-catchments in rejuvenated landscape.

3.3.3. Anthropogenic Controls

Over the 1986–2019 period, we observed an increase in agricultural land at the expense of forest and rangeland (Figure 9). However, the pattern is contrasting between the different catchments, with the largest increase in agricultural land in the Sile and Elgo (~32% each), and more forests in the Shafe and Basso. In the Shafe, Basso and Sile, the largest percentages of severely to extremely degraded active gullies occur in stable agricultural land, mostly within rejuvenated landscapes (Figure 9). In the Elgo, the largest percentage is in a zone of agriculture expansion, which is also located in the rejuvenated landscape. For inactive gullies, the largest percentages of severely to extremely degraded areas occur in stable agricultural land of the Shafe and Elgo, and in the zone of rangeland expansion for Sile.

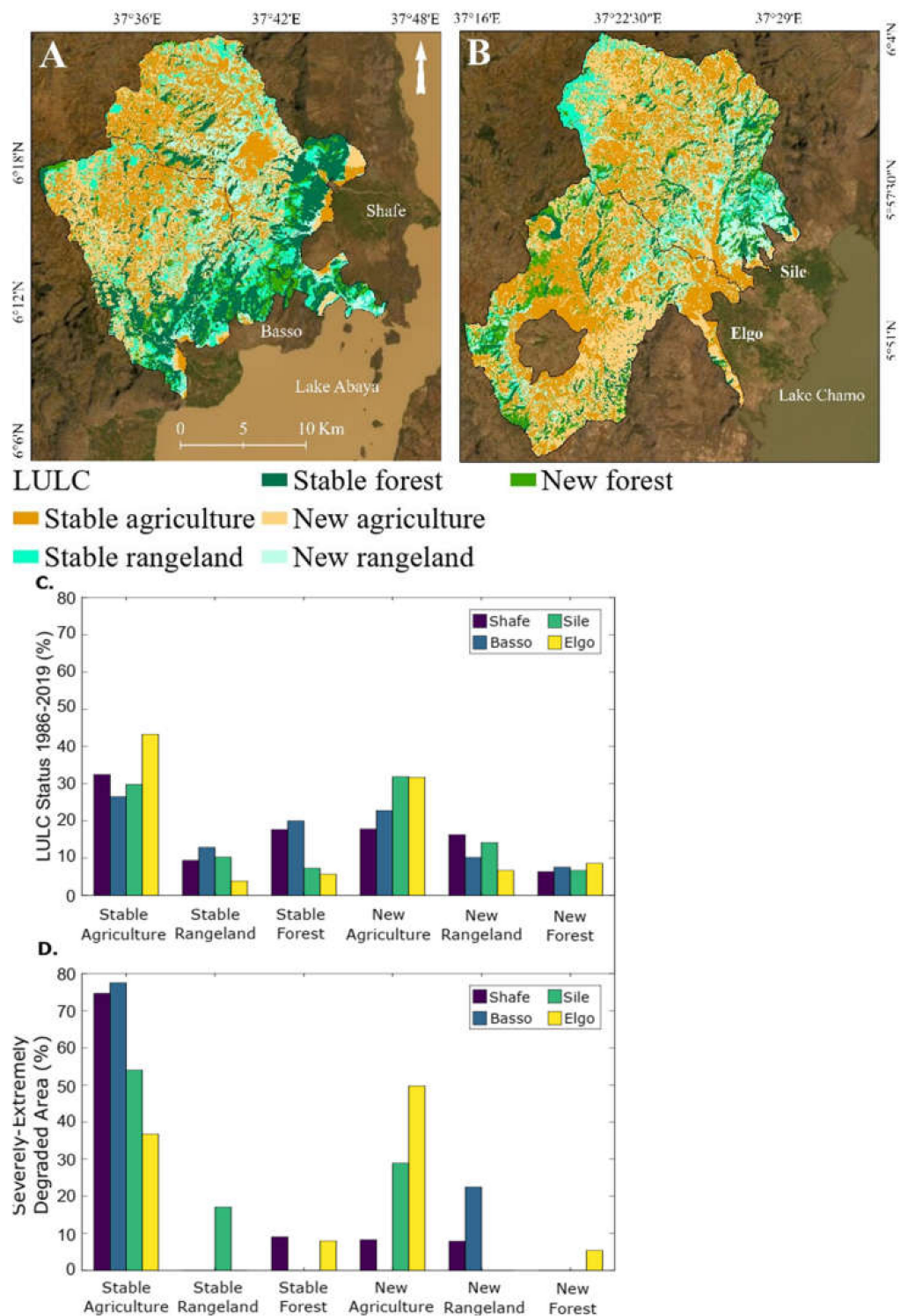


Figure 9. Relationship between LULC dynamics over the 1986–2019 period and severity of degraded area based on GLD (i.e., $GLD > 1 \text{ km km}^{-2}$) for each study catchment. (A) LULC dynamics of Shafe and Basso, and (B) Sile and Elgo catchments. (C) Percentage of each LULC that remained unchanged or that was gained for each catchment. (D) Percentage of area covered by severe to extreme degradation for each LULC using active gullies. Most of the severely and extremely degraded sub-catchments of Shafe and Basso, and all sub-catchments of Sile and Elgo are located in rejuvenated landscapes.

A total of ~340,000 people were living in the area in 2020 [71], resulting in a high average population density ($310 \text{ inhabitants km}^{-2}$) for a rural landscape. Higher population

densities are observed on flatter slopes $<10^\circ$, at elevations <1300 m and >1800 m; however, agricultural activities are common in the steeper midlands of the study catchments. Overall, there is an inverse relationship between population density and GLD; although in the Shafe, several populated sub-catchments are more prone to gullying (Appendix A Figure A4).

Overall, road density and GLD show an inverse relationship for the Shafe and Sile, whereas no clear relationship is observed for the Basso and Elgo. Road density, similar to the population density, is higher in the lowlands and upper plateau where fewer gullies are observed. In the different catchments, 6–25% of the gullies are connected to the roads (Table 1) and half of the gullies connected to roads are active; i.e., a proportion of activity similar to that observed for the whole gully inventory.

3.3.4. Landslides

Seventeen percent of landslides are characterized by gully incision. These landslides host more than 1200 gullies (Table 3) within the older and larger landslides. In the Basso and Sile, two of the largest landslides host over 100 gullies each. Some examples of gullies observed within the landslide are shown in Figure 4, including active and partially active gullies. As exemplified in Figure 4, we commonly observe that gullies affect the “head” of the slide where steep slopes are formed by depletion, but also the toe (convex steep slope formed by accumulation of landslide debris) or the lateral edge of the slide (flow convergence). The proportions of gullies within and outside the landslides vary among the different landscapes (Table 3). In the rejuvenated landscapes of all catchments, the proportions of active gullies (both number and length) are much higher within the landslides than outside. A similar trend was also observed for inactive gullies, except in the Shafe.

4. Discussion

4.1. Gully and Landslide Inventories, Data Reliability and Age of the Processes

We mapped a total of 7336 gullies and 430 landslides in an area of 871 km^2 —excluding the lowlands, flat zones and depression where no gullies and landslides developed. Google Earth imagery proved to be an effective mapping tool with errors of only 4% for gullies and 10% for landslides. This level of accuracy is similar or better than that reported in other studies using Google Earth imagery, for example [24,72–74].

Despite the high accuracy of the inventories, care must be taken with their reliability. Errors are mainly associated with small features or high vegetation cover preventing correct identification using Google Earth imagery. With respect to landslide activity, we identified two populations: active landslides that are relatively small and shallow, and large deep-seated landslides that are inactive. Small active landslides are slope-related processes whose signature in the landscape can disappear quickly, sometimes over a few years due to vegetation regeneration and land reclamation [75,76]. The oldest image in Google Earth used for the mapping being from 2016, we thus argue that the inventory of these small active failures provides information on the state of the landscape over a period of ~10 years. Our inventory is therefore insufficient to consider the role of extreme events with decadal return periods or human-induced landscape changes, for example [23,24,77]. Nevertheless, small landslides are clearly contemporary of the current natural and human-induced environmental conditions. The ages of large landslides are undetermined and clearly much older, potentially over 1 kyr [25], and have natural origins associated with environmental factors that have not been recorded during the last decade [78]. Although some of these large landslides show altered morphologies from erosion, we argue with confidence on the completeness of this inventory [13].

Overall, our landslide inventory provides information that complements two recent mapping efforts that only partially cover the study area [13,79]. The authors of [13] looked at a few rather large-scale and old landslides, whereas [79] investigated recent small-scale landslides. Note that the latter study provides an inventory that includes, under the name “landslide”, a lot of mass-movements that are distributed along gully banks and

therefore directly associated with the formation of these erosion processes. Such small-scale slope instabilities that we also observed in the field are not considered in our inventory as landslides since they are above all the direct consequence of soil erosion processes and respond to different drivers.

Our inventory of more than 7000 gullies is a reliable dataset to highlight spatial contrast in gully occurrence across the study catchments and identify potential factors controlling their spatial distribution. The gully inventory discriminates between (partially) active and inactive processes. When a gully is initiated, its extension can be very quick, reaching sometimes more than 100 m per year [17]. In some cases, gully extensions of more than one kilometre in a few decades have been reported by [80]. When a gully forms, it can remain active over several decades [76,81]. For active gullies, we therefore interpret most of them to correspond with current natural environmental conditions, although the timing of their initiation and rate of expansion remains unconstrained. Once a gully has stabilized, it can remain visible in the landscape for several thousands of years [36,82].

4.2. Interactions between River Incision, Landslides and Gullies

The role of faults in explaining the presence of large landslides has been highlighted in previous studies within the region [13,79]. Here, we further consider the seismotectonic control on the occurrence of old bedrock landslides through the analysis of the rejuvenated landscapes created by the upstream migration of fault-related knickpoints. Faults, fractures, knickpoint migration and landscape rejuvenation are parameters that act as environmental controls on bedrock landslides in other regions [31,34,83], including in the context of a rifting system such as the central portion of the western branch of the East African Rift [24,76].

Our research is one of the very few that clearly demonstrate the role of landslides as processes favoring the occurrence of gullies [20,27,76], especially over such a large region. Of course, we cannot ignore the role of landscape rejuvenation within the scheme of landslide-gully interaction. Indeed, regolith is needed for the development of gullies [33,36], with regolith thickness often thinner and less continuous on steeper slopes [37,63]. The reduction of regolith availability would be further exacerbated through the rejuvenation of the landscape [32,35] and, to some extent, the presence of bedrock landslides [34]. Based on this model, we would thus expect that GLD would be lower in rejuvenated landscapes. However, the opposite was observed, suggesting that an optimum balance between regolith availability and slope steepness in and outside the landslides is reached. In other words, the recent landscape is old enough for providing regolith conditions favorable to gullying.

The higher GLD in the rejuvenated landscapes could suggest that the hillslopes are not at threshold angles and that rates of regolith production outpace or have reached an equilibrium with the rates of erosion, despite the presence of the large bedrock landslides. In the Shafe, Sile and Elgo, we observed that the highest GLD occur overall in sub-catchments with slope values 15–25° (Figure 6), which are typically below the threshold angles [24,31,34,83]. Nevertheless, our analysis of slope-specific GLD showed that a clear relationship with slopes was not met in the study area (Figure 6); the GLD patterns did not show any clear tendency towards a spatial trend. Various reasons may exist for this non-linear behavior and require the disentangling of the characteristics of regolith, weathering and rock properties [34,63] that are unknown in the region. Furthermore, the role of human activities should not be ignored (see Section 4.3). Nevertheless, we argue that one reason for the presence of gullies on steep slopes in a rejuvenated context is that retreating knickpoints are developing in areas where the lithology is more prone to weathering and regolith formation. Drainage networks may develop in places where the lithology is more prone to incision [84] and, for example, the basalts and trachybasalts may display profiles with a rather higher degree of weathering [13]. The rejuvenation is also associated with the presence of active faults. More intense fracturing could not only favor bedrock river incision and landslide, but also lead to higher weathering [34,75,84].

4.3. The Role of Humans in the Occurrence of Gullies and Landslides

Due to population increase in the area, pressure on natural resources is increasing. For example, agricultural land is expanding at the expense of forest and rangeland. Large areas of severely to extremely degraded gullies were also observed in agricultural land, in the period 1986–2019. Their occurrence could be associated with the practice of annual crops and livestock breeding in the steeper midland zones, where the land remains bare during off seasons. This can result in soil crusting and sealing, which can contribute to high runoff generation [85]. Human activities might, therefore, contribute to the occurrence of active gullies, with the highest densities in agricultural land. Even though the ages of inactive and partially active gullies are undetermined, the role of human-induced environmental conditions on their initiation might be minimal; the landscape rejuvenation being a more likely factor controlling their distribution.

The occurrence of gullies and landslides along roads might be due to the slope modification during cut and fill or concentration of runoff water by the establishment of artificial drains and increased catchment area [27,86]. However, road density and GLD have an inverse relationship for the Shafe and Sile, and no clear association for the Basso and Elgo catchments. Despite this, the role of road construction should not be ignored, as new and large gullies are observed, mainly along the main road in the Elgo catchment.

4.4. Gullies and Landslides as Sediment Source

The GLD of 1.6 km km^{-2} in our study area highlights significant land degradation. This density is significantly higher than those reported in previous studies in Ethiopia and other parts of the world with similar climate, and LULC, for example [60,87,88] (see Table A1 in Appendix A). Although gully incision is quite severe in the area, the majority of GLD values do not reach the threshold value proposed by [89] for badland topography (i.e., gully number density $>70 \text{ km}^{-2}$ and $\text{GLD} > 10 \text{ km km}^{-2}$).

An average of 10 gullies per km^2 was measured in our study area, which is more than most areas mapped across the Horn of Africa [51], with the notable exception of the Afar region of north eastern Ethiopia and Eritrea where more than 50 gullies per km^2 are concentrated. When only active gullies are considered, the area is characterized by moderate and moderate to severe degradation. This suggests that a significant amount of soil may be transported from uplands to lowlands during intense rainfalls, as a high GLD has been shown to be associated to higher soil loss [90]. With 15–30% of active gullies connected to the river network, i.e., proportions that are higher than that typically found in other regions [52,53], the potential of gullies acting as direct sediment sources is high. Partially active gullies connected to a river have the potential to deliver eroded sediments directly to the river as well.

Compared to gullies, landslides are less frequent in the area in terms of number and current activity. Evidence of landslides affecting 15% of the area, however, highlights that this geomorphological process has played a significant role in shaping the landscape over geological timescales. Although in some cases, the legacy of large landslides on the sediment patterns may persist over thousands of years [91], the current contribution to the sediment budget by these landslides here is limited as they are all old features that look stabilized. This does not mean that new large landslides cannot occur, as has been reported in other regions [23,92]. Since our period of observation was short, we did not observe clusters of small landslides. In the Kivu rift, the authors of [25] observed clusters of more than 500 mostly shallow and highly mobile landslides associated with convective rainfall. When this happens, these shallow landslides can have a strong impact on sediment delivery over a period of years to decades [21]. In our study area, active landslides are limited to small scale instabilities along the rivers, representing direct sediment sources to the hydrological network. These are commonly debris avalanches that might be triggered by river erosion. In the absence of extreme landslide events associated with intense rainfall during the short period of observation, recent landslides appear to play a minor role in the current sediment dynamics, representing a limited volume of mobilized sediment.

Sediment produced by gullies and landslides disconnected from the channel network is locally stored, and might later be actively reworked through surface runoff, creep and debris flows [75,93]. For the current sediment deposition problem of both the Abaya and Chamo lakes, sediment contributed by gullies and landslides may be significant, as many active gullies and landslides connect to the rivers that feed these lakes. Further research is required to determine the amount of sediment that gully erosion and landslides contribute to the two lakes, and to quantify soil loss and the temporal dynamics of gully initiation, evolution and stabilization.

5. Conclusions

The present study demonstrates that satellite image analysis through Google Earth coupled with targeted field validation is an effective method for deriving an exhaustive inventory of gullies and landslides at regional scale. Identifying the spatial distribution of gullies and landslides, their level of activity and connectivity with rivers is critical for identifying the areas contributing most to sediment production. The proportion of active gullies in the study area is three times higher than inactive gullies, suggesting that land degradation through gullying is an active process in the studied catchments and may have expanded in recent years, although this needs to be confirmed by landscape reconstruction over the last decades. This is not the case for landslides, where only small features along rivers seem to be actively contributing to the sediment budget, whereas large, old landslides that show very little sign of activity appear to be preferential zones for gully development. These large, older landslides are natural in origin, and mainly controlled by landscape rejuvenation.

Our analysis across four catchments of similar size highlights large contrasts in GLD, reaching up to 10.6 km km^{-2} in the most affected places. High GLD is mainly noted in sub-catchments with average slopes steeper than 10° and a landscape rejuvenated by the upslope propagation of knickpoints. These gullies affect the soils formed in volcanic rock, mainly BTL and ITR, but further documentation of the lithological and pedological variations is required to further characterize their control on gully occurrence.

At a regional scale, the occurrence of gullies does not seem to correlate with human factors such as population and road density. The recent construction of a tarmac road across one of the studied catchments, however, has caused a series of new and highly dynamic gullies to form. High GLDs are observed in agricultural land; however, further work is needed to better constrain gully initiation and evolution in these areas. To quantify the contribution of gully erosion and landslides in the overall sediment budget of the catchments of lakes Abaya and Chamo, an in-depth understanding of the factors controlling the distribution and level of activity of gullies, as well as quantification of the total amount of sediment delivered by each river catchment, is essential. This is also required for identifying suitable mitigation and rehabilitation measures of the gullies and landslides, and to prevent increasing soil loss and its consequent sedimentation in the Abaya and Chamo Lakes.

Our study further demonstrates the important interactions between gullies and landslides. Although large landslides do not contribute to the current sediment budget, the high GD and GLD of active gullies within landslides show that they favor the development of gullies. Although less frequent, the presence of active landslides along the gully banks also shows that gully formation locally favors the initiation of shallow landslides.

Overall, the role of the large landslides, together with landscape rejuvenation, highlights the dominance of natural, long-term, geomorphological factors on land degradation processes. Our detailed inventory and characterization of these land degradation processes in the catchments of lakes Abaya and Chamo are a step towards understanding the natural and anthropic controls of sediment production, and a contribution to the long-term objective of more sustainable land management practices preserving soils and reducing sediment delivery to the lakes.

Author Contributions: L.B. conceived and design the study, carried out the data collection, data analysis, writing—original draft preparation, and review and editing. M.K. participated in conceptualization, methodology, writing—review and editing, supervision, and project administration. O.D. participated in conceptualization, data collection and validation, methodology, writing—review and editing, and supervision. J.P. and G.G. participated in writing—review and editing, and supervision. D.O., T.E. and A.K. participated in review and editing. All authors have read and agreed to the published version of the manuscript.

Funding: This research was funded by VLIR-UOS, in the framework of the Inter-University Cooperation with Arba Minch University.

Institutional Review Board Statement: Not applicable.

Informed Consent Statement: Not applicable.

Data Availability Statement: Not applicable.

Acknowledgments: We are very grateful to VLIR-UOS for supporting the PhD scholarship of Li-uelsegad Belayneh and the field research in the framework of the Inter-University Cooperation with Arba Minch University. Arba Minch University is acknowledged for its facilitation and logistic arrangement for this research work. The authors would like to acknowledge those who helped during fieldwork.

Conflicts of Interest: The authors declare no conflict of interest.

Appendix A

Table A1. Overview of GLD reported for different regions.

No.	Location	GLD (km km ⁻²)	Climate	Dominant LULC	Dominant Soil/Parent Material	Area (km ²)	Source
1	China, northeast	0.3–1.2	<i>Dwb</i>	Cropland	Luvic Phaeozem	28	[85]
2	China, northeast	0–72.0	<i>Dwb</i>	Cropland	Black, meadow, albic and dark brown soil	164	[94]
3	Latvia, south-east	0–4.5	<i>Dfb</i>	NA	Glacial, glacialfluvial and alluvial deposits	8423	[95]
4	Australia, north-central Victoria	<5.2	<i>Cfb</i>	Cropland and grazing land	Red/grey Vertisols, red Sodosols	3300	[52]
5	Australia, southeast	0.6–0.9	<i>Cfb</i>	Forest	NA	192	[72]
6	China, northeast	1.9–2.4	<i>Dwb</i>	Farmland	Mollisols with silty clay loam, high clay content and high SOM	24	[96]
7	DR Congo	0.4–2	<i>Aw</i>	Forest, few grasses	Sandy soils	443	[80]
8	Ethiopia, central	0.6–1.2	<i>Aw</i>	Cropland	Mollic Andosols	24	[87]
9	Ethiopia, central	0.7–1.1	<i>Aw</i>	Agriculture	Nitisols	5.4	[61]
10 *	Ethiopia, north	0.3–1	<i>Csb</i>	Cultivated land	Acrisols, Leptosols, Regosols, Luvisols, and Vertisols	21.5	[97]
11	Ethiopia, north	0.6–1.4	<i>Cwb</i>	Agriculture	Leptosols	12.6	[59]

Table A1. Cont.

No.	Location	GLD (km km ⁻²)	Climate	Dominant LULC	Dominant Soil/Parent Material	Area (km ²)	Source
12	Ethiopia, north	0–2.8	<i>BSh</i>	Cropland	Cambisols, Leptosols and Regosols	5142	[50]
13	Ethiopia, central	0.6–1.8	<i>Cwb</i>	Arable land	Leptosols	49.3	[98]
14	Ethiopia, south	0–10.6	<i>Aw</i>	Agriculture	Cambisols and Nitisols	756	This study
15	Ethiopia, south	0.5–1.7	<i>Aw</i>	Cropland	Regosols	5.7	[60]
16 *	Australia, north	0–8.3	<i>BSh, Cfa, Cwa</i>	NA	Luvisols, Regosols and Vertisols	85,000	[88]
17	Romania, Moldavia	0.1–3	<i>Dfb</i>	Agriculture	NA	25,000	[99]
18 *	Russia, East	0–4.2	<i>Dfb</i>	Cropland, mixed forest	Gray forest soils and medium leached chernozem	188,000	[100]
19 *	Russia, European territory	0–0.5	<i>Dfb, Dfa</i>	Arableland	Chalk, marls and sands	15	[101]

Notice: NA: no data for the area, SOM: soil organic matter. * Studies carried out in more than one catchment/region and therefore represent more than one climate, dominant land use, land cover or soil type. *Aw*: tropical savanna climate, *BSh*: hot semi-arid climate, *Cfa*: humid subtropical climate, *Cfb*: temperate oceanic climate, *Csb*: warm-summer Mediterranean climate, *Cwa*: monsoon-influenced humid subtropical climate, *Cwb*: subtropical highland climate or monsoon-influenced temperate oceanic climate, *Dfa*: hot-summer humid continental climate, *Dfb*: warm-summer humid continental climate, *Dwb*: monsoon-influenced warm-summer humid continental climate.

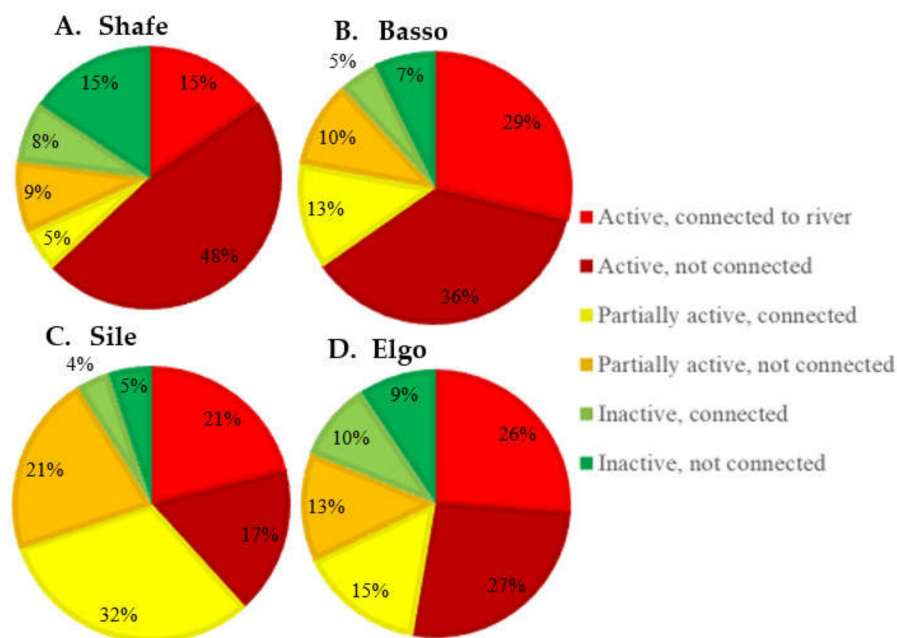


Figure A1. Activity status of gullies and their connectivity to the rivers for each catchment. Total number of gullies in Shafe, Basso, Sile and Elgo are 3640, 823, 1748 and 1125, respectively.

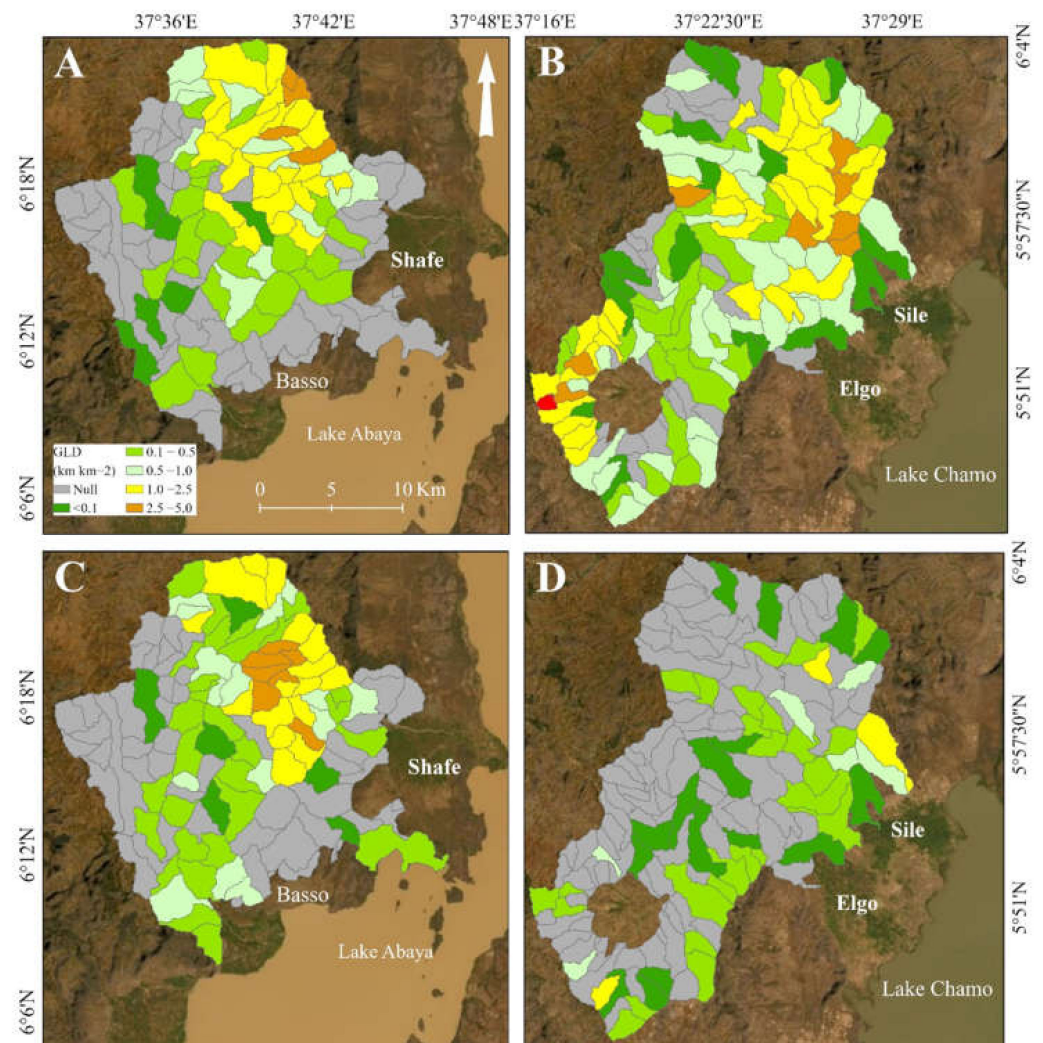


Figure A2. The GLD, for partially active (A,B) and inactive (C,D) gullies of each river catchment. The densities are represented at the level of the sub-catchments. Background imagery is from Google Earth (15 June 2020).

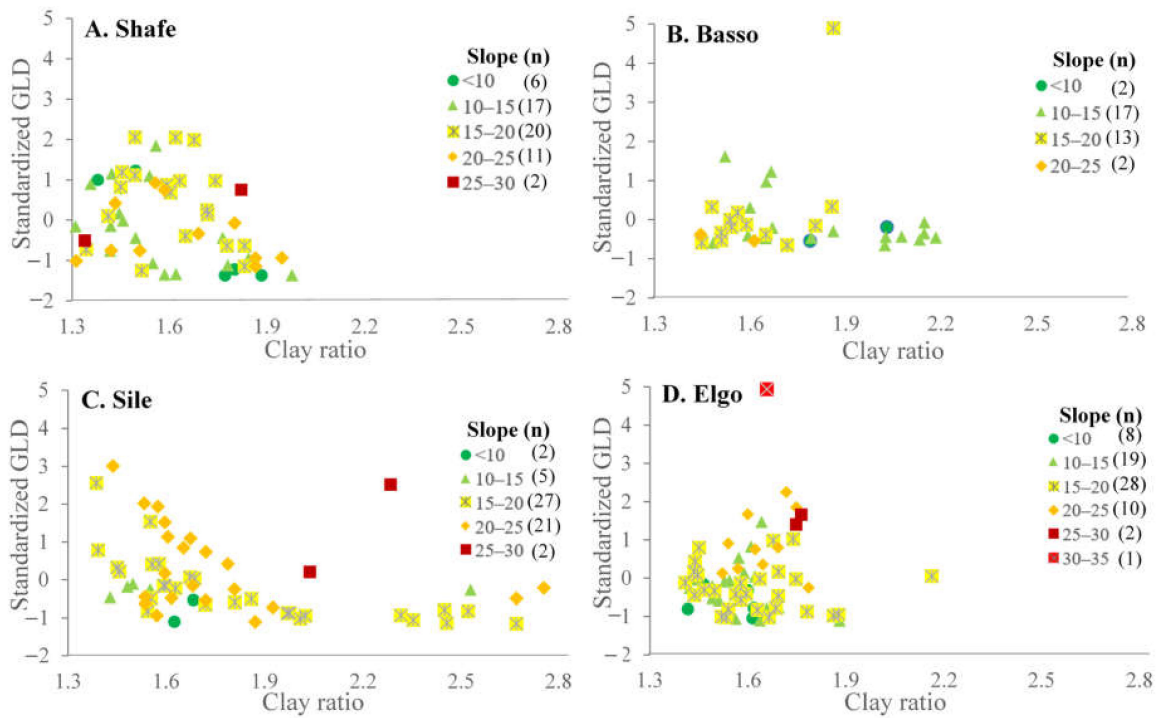


Figure A3. Relationships between GLD with clay ratio of the soil and slope angle for each sub-catchment of the four study catchments. Clay ratio is % (sand + silt)/% (clay). Slope represents the mean slope angle (degree) of each sub-catchment and n represents the number of sub-catchments for each slope-angle class.

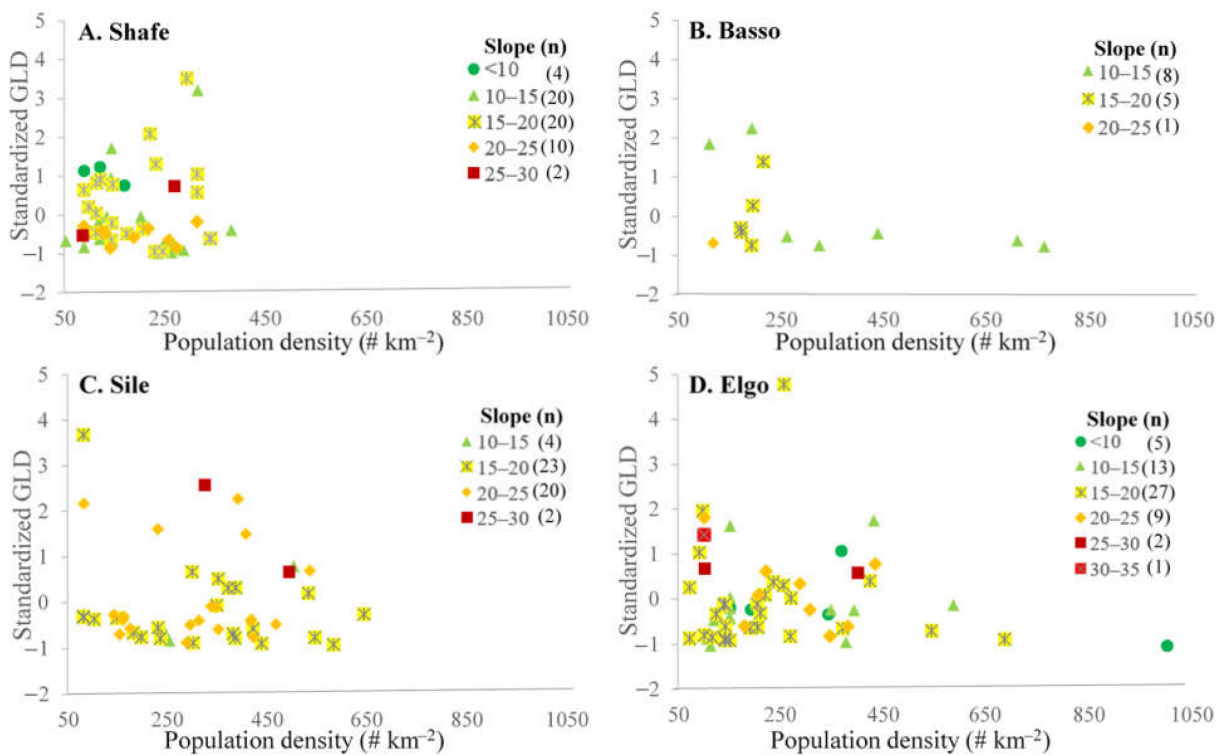


Figure A4. Relationships between population density for the year 2020 and GLD, for active gullies of each river catchment. Slope represents the mean slope angle (degree) of each sub-catchment and n represents the number of sub-catchments of each slope-angle class.

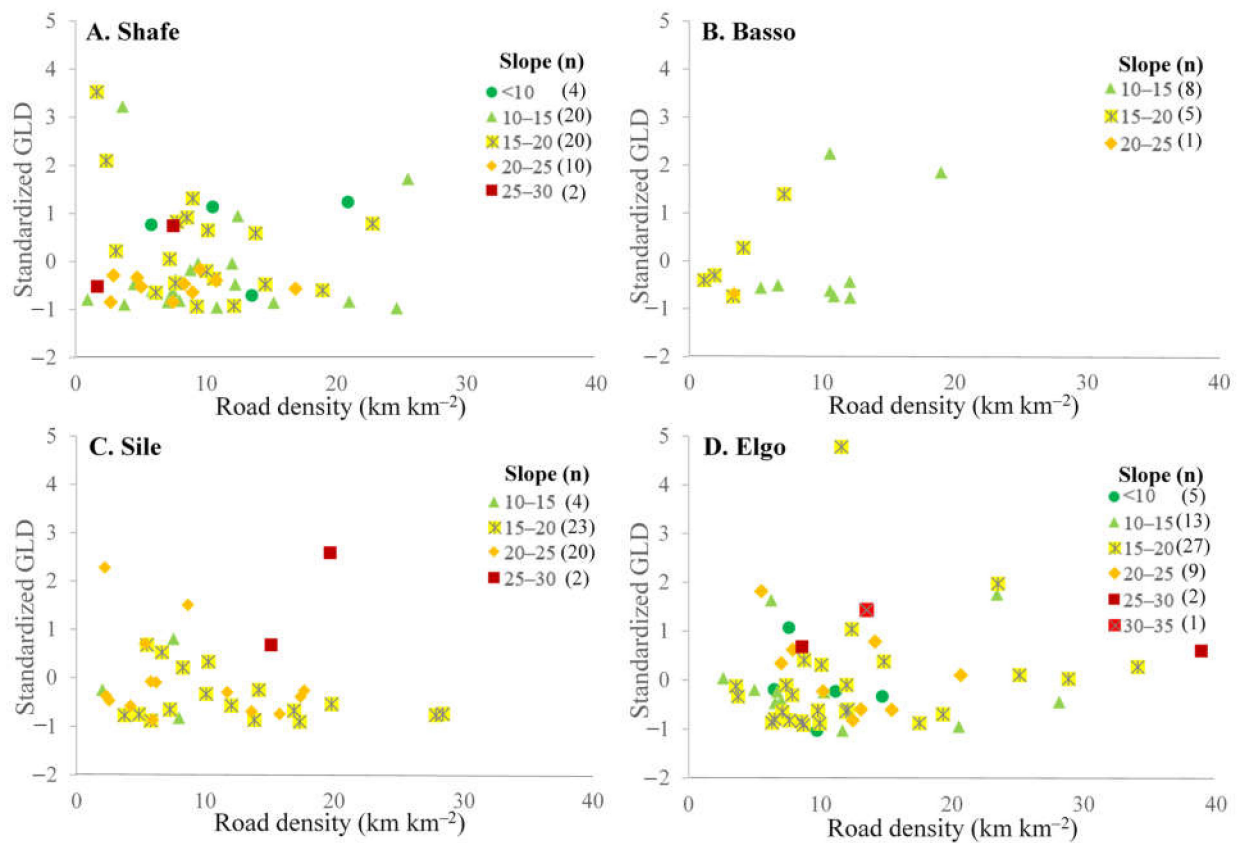


Figure A5. Relationships between road density and GLD, for active gullies of each river catchment. Slope represents the mean slope angle (degree) of each sub-catchment and n represents the number of sub-catchments of each slope-angle class.

References

- Donohue, I.; Garcia Molinos, J. Impacts of Increased Sediment Loads on the Ecology of Lakes. *Biol. Rev.* **2009**, *84*, 517–531. [[CrossRef](#)] [[PubMed](#)]
- Downing, J.A. Emerging Global Role of Small Lakes and Ponds: Little Things Mean a Lot. *Limnetica* **2010**, *29*, 9–24. [[CrossRef](#)]
- Verpoorter, C.; Kutser, T.; Seekell, D.A.; Tranvik, L.J. A Global Inventory of Lakes Based on High-Resolution Satellite Imagery. *Geophys. Res. Lett.* **2014**, *41*, 6396–6402. [[CrossRef](#)]
- Yang, X. *Manual on Sediment Management and Measurement*; World Meteorological Organization Operational Hydrology Report No. 47; Secretariat of the World Meteorological Organization: Geneva, Switzerland, 2003; ISBN 9263109486.
- Syvitski, J.P.M.; Vörösmarty, C.J.; Kettner, A.J.; Green, P. Impact of Humans on the Flux of Terrestrial Sediment to the Global Coastal Ocean. *Science* **2005**, *308*, 376–380. [[CrossRef](#)]
- Olago, D.O.; Odada, E.O. Sediment Impacts in Africa's Transboundary Lake/River Basins: Case Study of the East African Great Lakes. *Aquat. Ecosyst. Health Manag.* **2007**, *10*, 23–32. [[CrossRef](#)]
- Ayenew, T.; Legesse, D. The Changing Face of the Ethiopian Rift Lakes and Their Environs: Call of the Time. *Lakes Reserv. Res. Manag.* **2007**, *12*, 149–165. [[CrossRef](#)]
- Belete, M.D.; Hebart-Coleman, D.; Mathews, R.E.; Zazu, C. Building Foundations for Source-to-Sea Management: The Case of Sediment Management in the Lake Hawassa Sub-Basin of the Ethiopian Rift Valley. *Water Int.* **2021**, *46*, 138–156. [[CrossRef](#)]
- Schütt, B.; Thiemann, S. Kulfo River, South Ethiopia as a Regulator of Lake Level Changes in the Lake Abaya-Lake Chamo System. *Zbl. Geol. Paläont.* **2006**, *1*, 129–143.
- Teffera, F.E. The Ecology of the Major Ethiopian Rift Valley Lakes Abaya and Chamo, with Special Reference to Water Quality and Food Web Structure. Ph.D. Thesis, KU Leuven, Leuven, Belgium, 2016.
- Schütt, B.; Förch, G.; Bekele, S.; Thiemann, S. Modern Water Level and Sediment Accumulation Changes of Lake Abaya, Southern Ethiopia—A Case Study from the Northern Lake Area. *Water Res. Environ.* **2002**, *2*, 418–422.
- Assefa, E. Landscape Dynamics and Sustainable Land Management in Southern Ethiopia. Ph.D. Thesis, Christian-Albrechts-Universität Zu Kiel, Kiel, Germany, 2012.

13. Martínek, K.; Verner, K.; Hroch, T.; Megerssa, L.; Kopačková, V.; Buriánek, D.; Muluneh, A.; Kalinová, R.; Yakob, M.; Kassa, M. Main Ethiopian Rift Landslides Formed in Contrasting Geological Settings and Climatic Conditions. *Nat. Hazards Earth Syst. Sci.* **2021**, *21*, 3465–3487. [[CrossRef](#)]
14. Shi-Biao, B.; Wang, J.; Lü, G.; Zhou, P.; Hou, S.; Xu, S.-N. GIS-Based Logistic Regression for Landslide Susceptibility Mapping of the Zhongxian Segment in the Three Gorges Area, China. *Geomorphology* **2010**, *115*, 23–31. [[CrossRef](#)]
15. Ost, L.; van den Eeckhaut, M.; Poesen, J.; Vanmaercke-Gottigny, M.C. Characteristics and Spatial Distribution of Large Landslides in the Flemish Ardennes (Belgium). *Z. Geomorphol.* **2003**, *47*, 329–350. [[CrossRef](#)]
16. Valentin, C.; Poesen, J.; Li, Y. Gully Erosion: Impacts, Factors and Control. *Catena* **2005**, *63*, 132–153. [[CrossRef](#)]
17. Vanmaercke, M.; Poesen, J.; Van Mele, B.; Demuzere, M.; Bruynseels, A.; Golosov, V.; Rodrigues Bezerra, J.; Bolysov, S.; Dvinskih, A.; Frankl, A.; et al. How Fast Do Gully Headcuts Retreat? *Earth-Sci. Rev.* **2016**, *154*, 336–355. [[CrossRef](#)]
18. Poesen, J.; Nachtergaele, J.; Verstraeten, G.; Valentin, C. Gully Erosion and Environmental Change: Importance and Research Needs. *Catena* **2003**, *50*, 91–133. [[CrossRef](#)]
19. Chesworth, W. *Slope Classes. Encyclopedia of Soil Science; Encyclopedia of Earth Sciences Series*; Springer: Dordrecht, The Netherlands, 2008. [[CrossRef](#)]
20. Mackey, B.H.; Roering, J.J. Sediment Yield, Spatial Characteristics, and the Long-Term Evolution of Active Earthflows Determined from Airborne LiDAR and Historical Aerial Photographs, Eel River, California. *Bull. Geol. Soc. Am.* **2011**, *123*, 1560–1576. [[CrossRef](#)]
21. Whipp, D.M.; Ehlers, T.A. Quantifying Landslide Frequency and Sediment Residence Time in the Nepal Himalaya. *Sci. Adv.* **2019**, *5*, eaav348. [[CrossRef](#)]
22. Sidle, R.C.; Bogaard, T.A. Dynamic Earth System and Ecological Controls of Rainfall-Initiated Landslides. *Earth-Sci. Rev.* **2016**, *159*, 275–291. [[CrossRef](#)]
23. Marc, O.; Behling, R.; Andermann, C.; Turowski, J.M.; Illien, L.; Roessner, S.; Hovius, N. Long-Term Erosion of the Nepal Himalayas by Bedrock Landsliding: The Role of Monsoons, Earthquakes and Giant Landslides. *Earth Surf. Dyn.* **2019**, *7*, 107–128. [[CrossRef](#)]
24. Depicker, A.; Govers, G.; Jacobs, L.; Campforts, B.; Uwihirwe, J.; Dewitte, O. Interactions between Deforestation, Landscape Rejuvenation, and Shallow Landslides in the North Tanganyika-Kivu Rift Region, Africa. *Earth Surf. Dyn.* **2021**, *9*, 445–462. [[CrossRef](#)]
25. Dewitte, O.; Dille, A.; Depicker, A.; Kubwimana, D.; Maki Mateso, J.C.; Mugaruka Bibentyo, T.; Uwihirwe, J.; Monsieurs, E. Constraining Landslide Timing in a Data-Scarce Context: From Recent to Very Old Processes in the Tropical Environment of the North Tanganyika-Kivu Rift Region. *Landslides* **2021**, *18*, 161–177. [[CrossRef](#)]
26. Nyssen, J.; Moeyersons, J.; Poesen, J.; Deckers, J.; Haile, M. The Environmental Significance of the Remobilisation of Ancient Mass Movements in the Atbara—Tekeze Headwaters, Northern Ethiopia. *Geomorphology* **2002**, *49*, 303–322. [[CrossRef](#)]
27. Poesen, J. Soil Erosion in the Anthropocene: Research Needs. *Earth Surf. Processes Landf.* **2018**, *43*, 64–84. [[CrossRef](#)]
28. Corti, G. Continental Rift Evolution: From Rift Initiation to Incipient Break-up in the Main Ethiopian Rift, East Africa. *Earth-Sci. Rev.* **2009**, *96*, 1–53. [[CrossRef](#)]
29. Saria, E.; Calais, E.; Stamps, D.S.; Delvaux, D.; Hartnady, C.J.H. Present-Day Kinematics of the East African Rift. *J. Geophys. Res. Solid Earth* **2014**, *119*, 3584–3600. [[CrossRef](#)]
30. Larsen, M.C. Landslides and Sediment Budgets in Four Watersheds in Eastern Puerto Rico. In *Water Quality and Landscape Processes of Four Watersheds in Eastern Puerto Rico*; USGS: Reston, VA, USA, 2012; pp. 153–178.
31. Bennett, G.L.; Miller, S.R.; Roering, J.J.; Schmidt, D.A. Landslides, Threshold Slopes, and the Survival of Relict Terrain in the Wake of the Mendocino Triple Junction. *Geology* **2016**, *44*, 363–366. [[CrossRef](#)]
32. Schoenbohm, L.M.; Whipple, K.X.; Burchfiel, B.C.; Chen, L. Geomorphic Constraints on Surface Uplift, Exhumation, and Plateau Growth in the Red River Region, Yunnan Province, China. *Bull. Geol. Soc. Am.* **2004**, *116*, 895–909. [[CrossRef](#)]
33. Menéndez-Duarte, R.; Marquínez, J.; Fernández-Menéndez, S.; Santos, R. Incised Channels and Gully Erosion in Northern Iberian Peninsula: Controls and Geomorphic Setting. *Catena* **2007**, *71*, 267–278. [[CrossRef](#)]
34. Clarke, B.A.; Burbank, D.W. Quantifying Bedrock—Fracture Patterns within the Shallow Subsurface: Implications for Rock Mass Strength, Bedrock Landslides, and Erodibility. *J. Geophys. Res. Earth Surf.* **2011**, *116*, F04009. [[CrossRef](#)]
35. Braun, J.; Mercier, J.; Guillocheau, F.; Robin, C. A Simple Model for Regolith Formation by Chemical Weathering. *J. Geophys. Res. Earth Surf.* **2016**, *121*, 2140–2171. [[CrossRef](#)]
36. Brosens, L.; Broothaerts, N.; Campforts, B.; Jacobs, L.; Razanamahandry, V.F.; Van Moerbeke, Q.; Bouillon, S.; Razafimbelo, T.; Rafolisy, T.; Govers, G. Under Pressure: Rapid Lavaka Erosion and Floodplain Sedimentation in Central Madagascar. *Sci. Total Environ.* **2022**, *806*, 150483. [[CrossRef](#)] [[PubMed](#)]
37. Brosens, L.; Campforts, B.; Robinet, J.; Vanacker, V.; Opfergelt, S.; Ameijeiras-Mariño, Y.; Minella, J.P.G.; Govers, G. Slope Gradient Controls Soil Thickness and Chemical Weathering in Subtropical Brazil: Understanding Rates and Timescales of Regional Soilscape Evolution Through a Combination of Field Data and Modeling. *J. Geophys. Res. Earth Surf.* **2020**, *125*, e2019JF005321. [[CrossRef](#)]
38. Bonini, M.; Corti, G.; Innocenti, F.; Manetti, P.; Mazzarini, F.; Abebe, T.; Pecskey, Z. Evolution of the Main Ethiopian Rift in the Frame of Afar and Kenya Rifts Propagation. *Tectonics* **2005**, *24*, TC1007. [[CrossRef](#)]

39. Molin, P.; Corti, G. Topography, River Network and Recent Fault Activity at the Margins of the Central Main Ethiopian Rift (East Africa). *Tectonophysics* **2015**, *664*, 67–82. [[CrossRef](#)]
40. Minda, T.T.; van der Molen, M.K.; Struik, P.C.; Combe, M.; Jiménez, P.A.; Khan, M.S.; de Arellano, J.V.G. The Combined Effect of Elevation and Meteorology on Potato Crop Dynamics: A 10-Year Study in the Gamo Highlands, Ethiopia. *Agric. For. Meteorol.* **2018**, *262*, 166–177. [[CrossRef](#)]
41. MOWR. *Rift Valley Lakes Basin Integrated Resources Development Master Plan Study Project. Part II Prefeasibility Studies*; Federal Democratic Republic of Ethiopia, Ministry of Water Resources: Addis Ababa, Ethiopia, 2010; (unpublished).
42. Teffera, F.; Lemmens, P.; Deriemaecker, A.; Brendonck, L.; Dondeyne, S.; Deckers, J.; Bauer, H.; Gamo, F.W.; Meester, L.D. A Call to Action: Strong Long-Term Limnological Changes in the Two Largest Ethiopian Rift Valley Lakes, Abaya and Chamo. *Inland Waters* **2017**, *2041*, 129–137. [[CrossRef](#)]
43. Beck, H.E.; Zimmermann, N.E.; McVicar, T.R.; Vergopolan, N.; Berg, A.; Wood, E.F. Present and Future Köppen-Geiger Climate Classification Maps at 1-Km Resolution. *Sci. Data* **2018**, *5*, 180214. [[CrossRef](#)]
44. Assefa, E.; Bork, H. Dynamics and Driving Forces of Agricultural Landscapes in Southern Ethiopia—A Case Study of the Chencha and Arbaminch Areas. *J. Land Use Sci.* **2017**, *11*, 278–293. [[CrossRef](#)]
45. Wagesho, N. Catchment Dynamics and Its Impact on Runoff Generation: Coupling Watershed Modelling and Statistical Analysis to Detect Catchment Responses. *Int. J. Water Resour. Environ. Eng.* **2015**, *6*, 73–87. [[CrossRef](#)]
46. NMA. Dekadal Rainfall. Adjusted Rainfall Reconstruction Data. Ethiopian National Meteorological Agency. 2020. Available online: <https://iridl.ldeo.columbia.edu/SOURCES/.Ethiopia/> (accessed on 14 May 2020).
47. Dewitte, O.; Jones, A.; Elbelrhiti, H.; Horion, S.; Montanarella, L. Satellite Remote Sensing for Soil Mapping in Africa: An Overview. *Prog. Phys. Geogr.* **2012**, *36*, 514–538. [[CrossRef](#)]
48. Guzzetti, F.; Mondini, A.C.; Cardinali, M.; Fiorucci, F.; Santangelo, M.; Chang, K.T. Landslide Inventory Maps: New Tools for an Old Problem. *Earth-Sci. Rev.* **2012**, *112*, 42–66. [[CrossRef](#)]
49. Desprats, J.F.; Raclot, D.; Rousseau, M.; Cerdan, O.; Garcin, M.; Bissonnais, Y.L.E.; Slimane, A.B.E.N.; Fouche, J. Mapping Linear Erosion Features Using High and Very High Resolution Satellite Imagery. *Land Degrad. Dev.* **2013**, *32*, 22–32. [[CrossRef](#)]
50. Guyassa, E.; Frankl, A.; Zenebe, A.; Poesen, J.; Nyssen, J. Gully and Soil and Water Conservation Structure Densities in Semi-Arid Northern Ethiopia over the Last 80 Years. *Earth Surf. Processes Landf.* **2018**, *43*, 1848–1859. [[CrossRef](#)]
51. Vanmaercke, M.; Chen, Y.; Haregeweyn, N.; De Geeter, S.; Campforts, B.; Heyndrickx, W.; Tsunekawa, A.; Poesen, J. Predicting Gully Densities at Sub-Continental Scales: A Case Study for the Horn of Africa. *Earth Surf. Processes Landf.* **2020**, *45*, 3763–3779. [[CrossRef](#)]
52. Whitford, J.A.; Newham, L.T.H.; Vigiak, O.; Melland, A.R.; Roberts, A.M. Geomorphology Rapid Assessment of Gully Sidewall Erosion Rates in Data-Poor Catchments: A Case Study in Australia. *Geomorphology* **2010**, *118*, 330–338. [[CrossRef](#)]
53. Zhang, W.; Liu, Y. Research on Visual Interpretation and Spatial Distribution Pattern of the Erosion Gully in Luoyugou Watershed of China. *Environ. Nat. Resour. Res.* **2019**, *9*, 23–31. [[CrossRef](#)]
54. WP/WLI International Geotechnical Societies' UNESCO Working Party on World Landslide. A Suggested Method for Describing the Activity of a Landslide. *Int. Assoc. Eng. Geol. Bull.* **1993**, *47*, 53–57. [[CrossRef](#)]
55. Keaton, J.R.; Degraff, J.V. Surface Observation and Geologic Mapping. *Spec. Rep.-Natl. Res. Council. Transp. Res. Board* **1996**, *247*, 178–230.
56. Marden, M.; Betts, H.; Arnold, G.; Hambling, R. Gully Erosion and Sediment Load: Waipaoa, Waiapu and Uawa Rivers, Eastern North Island, New Zealand. In Proceedings of the 2008 Symposium of the International Commission on Continental Erosion, Christchurch, New Zealand, 1–5 December 2008; pp. 339–350.
57. Conoscenti, C.; Angileri, S.; Cappadonia, C.; Rotigliano, E.; Agnesi, V.; Märker, M. Gully Erosion Susceptibility Assessment by Means of GIS-Based Logistic Regression: A Case of Sicily (Italy). *Geomorphology* **2014**, *204*, 399–411. [[CrossRef](#)]
58. Jacobs, L.; Kervyn, M.; Reichenbach, P.; Rossi, M.; Marchesini, I.; Alvioli, M.; Dewitte, O. Regional Susceptibility Assessments with Heterogeneous Landslide Information: Slope Unit- vs. Pixel-Based Approach. *Geomorphology* **2020**, *356*, 107084. [[CrossRef](#)]
59. Addisu, S. Assessment of the Impact of Road Construction on Physical Land Degradation in Central Highlands of Ethiopia. Master's Thesis, Addis Ababa University, Addis Ababa, Ethiopia, 2009.
60. Belayneh, L.; Bantider, A.; Moges, A. Road Construction and Gully Development in Hadero Tunto-Durgi Road Project, Southern Ethiopia. *Ethiop. J. Environ. Stud. Manag.* **2014**, *7*, 720. [[CrossRef](#)]
61. Osore, A.; Moges, A. Extent of Gully Erosion and Farmer's Perception of Soil Erosion in Alalicha Watershed, Southern Ethiopia. *J. Environ. Earth Sci.* **2014**, *4*, 74–82.
62. Hopp, L.; McDonnell, J.J. Connectivity at the Hillslope Scale: Identifying Interactions between Storm Size, Bedrock Permeability, Slope Angle and Soil Depth. *J. Hydrol.* **2009**, *376*, 378–391. [[CrossRef](#)]
63. Prancevic, J.P.; Lamb, M.P.; McArdell, B.W.; Rickli, C.; Kirchner, J.W. Decreasing Landslide Erosion on Steeper Slopes in Soil-Mantled Landscapes. *Geophys. Res. Lett.* **2020**, *47*, e2020GL087505. [[CrossRef](#)]
64. Schwanghart, W.; Scherler, D. Bumps in River Profiles: Uncertainty Assessment and Smoothing Using Quantile Regression Techniques. *Earth Surf. Dyn.* **2017**, *5*, 821–839. [[CrossRef](#)]
65. Yismaw, A.; Mitiku, B.; Beyene, B.; Gtsadik, T.; Dure, T.; Zewde, T.; Theshome, Y.; Tesfaye, W.; Abrham, R. *Geological Map of Dila Map Sheet (NB37-6)*; Federal Democratic Republic of Ethiopia Ministry of Mine, Geological Survey of Ethiopia: Addis Ababa, Ethiopia, 2012.

66. Hengl, T.; De Jesus, J.M.; Heuvelink, G.B.M.; Gonzalez, M.R. SoilGrids250m: Global Gridded Soil Information Based on Machine Learning. *PLoS ONE* **2017**, *12*, e0169748. [[CrossRef](#)]
67. Hua, A.K.; Ping, O.W. The Influence of Land-Use/Land-Cover Changes on Land Surface Temperature: A Case Study of Kuala Lumpur Metropolitan City. *Eur. J. Remote Sens.* **2018**, *51*, 1049–1069. [[CrossRef](#)]
68. USA National Geospatial-Intelligence Agency (NGA). *USGS Shuttle Radar Topography Mission, Digital Elevation Model 1 Arc-Second*; USA National Geospatial-Intelligence Agency (NGA): Springfield, VA, USA, 2000.
69. Bhandari, A. Feature Scaling for Machine Learning: Understanding the Difference between Normalization vs. Standardization. 2020. Available online: <https://www.analyticsvidhya.com/blog/2020/04/feature-scaling-machine-learning-normalization-standardization/> (accessed on 6 January 2022).
70. Olaniya, M.; Bora, P.K.; Das, S.; Chanu, P.H. Soil Erodibility Indices under Different Land Uses in Ri-Bhoi District of Meghalaya (India). *Sci. Rep.* **2020**, *10*, 114986. [[CrossRef](#)]
71. GZAD: Gamo Zone Agricultural Department. *Population Data of All Woredas and Kebeles of Gamo Zone*; GZAD: Arba Minch, Ethiopia, 2020; (Unpublished work).
72. McInnes, J.; Vigiak, O.; Roberts, A.M. Using Google Earth to Map Gully Extent in the West Gippsland Region (Victoria, Australia). In Proceedings of the MODSIM2011, The 19th International Congress on Modelling and Simulation, Perth, WA, Australia, 12–16 December 2011; pp. 3370–3376.
73. Frankl, A.; Poesen, J.; Haile, M.; Deckers, J.; Nyssen, J. Quantifying Long-Term Changes in Gully Networks and Volumes in Dryland Environments: The Case of Northern Ethiopia. *Geomorphology* **2013**, *201*, 254–263. [[CrossRef](#)]
74. Farooq, S.; Khan, M. *Preparing Landslide Inventory Maps Using Virtual Globes Introduction: Mohd*; Department of Geology, AMU: Uttar Pradesh, India, 2016; pp. 1–6.
75. Dewitte, O.; Depicker, A.; Moeyersons, J.; Dille, A. *Mass Movements in Tropical Climates*; Treatise on Geomorphology; Shroder, J.J.F., Ed.; Elsevier: Amsterdam, The Netherlands, 2022; Volume 5, pp. 338–349, ISBN 9780128182345.
76. Kubwimana, D.; Ait Brahim, L.; Nkurunziza, P.; Dille, A.; Depicker, A.; Nahimana, L.; Abdelouafi, A.; Dewitte, O. Characteristics and Distribution of Landslides in the Populated Hillslopes of Bujumbura, Burundi. *Geosciences* **2021**, *11*, 259. [[CrossRef](#)]
77. Depicker, A.; Jacobs, L.; Delvaux, D.; Havenith, H.-B.; Maki Mateso, J.-C.; Govers, G.; Dewitte, O. The Added Value of a Regional Landslide Susceptibility Assessment: The Western Branch of the East African Rift. *Geomorphology* **2020**, *353*, 106886. [[CrossRef](#)]
78. Maki Mateso, J.-C.; Biolders, C.; Monsieurs, E.; Depicker, A.; Smets, B.; Tambala, T.; Bagalwa Mateso, L.; Dewitte, O. Natural and Human-Induced Landslides in a Tropical Mountainous Region: The Rift Flank West of Lake Kivu (DR Congo). *Nat. Hazards Earth Syst. Sci. Discuss.* **2021**, *2021*, 1–35. [[CrossRef](#)]
79. Shano, L.; Raghuvanshi, T.K.R.; Meten, M. Landslide Hazard Zonation Using Logistic Regression Model: The Case of Shafe and Baso Catchments, Gamo Highland, Southern Ethiopia. *Geotech. Geol. Eng.* **2021**, *40*, 83–101. [[CrossRef](#)]
80. Makanzu Imwangana, F.; Dewitte, O.; Ntombi, M.; Moeyersons, J. Topographic and Road Control of Mega-Gullies in Kinshasa (DR Congo). *Geomorphology* **2014**, *217*, 131–139. [[CrossRef](#)]
81. Frankl, A.; Nyssen, J.; De Dapper, M.; Haile, M.; Billi, P.; Munro, R.N.; Deckers, J.; Poesen, J. Linking Long-Term Gully and River Channel Dynamics to Environmental Change Using Repeat Photography (Northern Ethiopia). *Geomorphology* **2011**, *129*, 238–251. [[CrossRef](#)]
82. Schmidtchen, G.; Bork, H.R. Changing Human Impact during the Period of Agriculture in Central Europe. The Case Study Biesdorfer Kehlen, Brandenburg, Germany. In *Long Term Hillslope and Fluvial System Modelling/Concepts and Case Studie*; Lang, A., Hennrich, K., Dikau, R., Eds.; Springer: Berlin/Heidelberg, Germany, 2003. [[CrossRef](#)]
83. Larsen, I.J.; Montgomery, D.R. Landslide Erosion Coupled to Tectonics and River Incision. *Nat. Geosci.* **2012**, *5*, 468–473. [[CrossRef](#)]
84. Campforts, B.; Vanacker, V.; Herman, F.; Vanmaercke, M.; Schwanghart, W.; Tenorio, G.E.; Willems, P.; Govers, G. Parameterization of River Incision Models Requires Accounting for Environmental Heterogeneity: Insights from the Tropical Andes. *Earth Surf. Dyn.* **2020**, *8*, 447–470. [[CrossRef](#)]
85. Zhang, T.; Liu, G.; Duan, X.; Wilson, G. V Spatial Distribution and Morphologic Characteristics of Gullies in the Black Soil Region of Northeast China: Hebei Watershed. *Phys. Geogr.* **2016**, *37*, 228–250. [[CrossRef](#)]
86. Nyssen, J.; Poesen, J.; Moeyersons Layeten, E.; Veyret-Picot, M.; Deckers, J.; Haile, M.; Govers, G. Impact of Road Building on Gully Erosion Risk: A Case Study from the Northern Ethiopian Highlands. *Earth Surf. Processes Landf.* **2002**, *1283*, 1267–1283. [[CrossRef](#)]
87. Moges, A.; Holden, N.M. Land Cover Change and Gully Development Between 1965 and 2000 in Umbulo Catchment, Ethiopia. *Mt. Res. Dev.* **2009**, *29*, 265–276. [[CrossRef](#)]
88. Darr, S.D.; Pringle, M.J. Improving Gully Density Maps for Modelling Water Quality within Great Barrier Reef Catchments. In Proceedings of the 22nd International Congress on Modelling and Simulation, Hobart, TAS, Australia, 3–8 December 2017; pp. 1920–1926.
89. Zachar, D. *Classification of Soil Erosion. Soil Erosion*; Elsevier Scientific Publishing Company: Amsterdam, The Netherlands, 1982.
90. Na, J.; Yang, X.; Tang, G.; Dang, W.; Strobl, J. Population Characteristics of Loess Gully System in the Loess Plateau of China. *Remote Sens.* **2020**, *12*, 2639. [[CrossRef](#)]
91. Korup, O.; Densmore, A.L.; Schlunegger, F. The Role of Landslides in Mountain Range Evolution. *Geomorphology* **2010**, *120*, 77–90. [[CrossRef](#)]

92. Dille, A.; Kervyn, F.; Mugaruka Bibentyo, T.; Delvaux, D.; Bamulezi Ganza, G.; Ilombe Mawe, G.; Kalikone Buzera, C.; Safari Nakito, E.; Moeyersons, J.; Monsieurs, E.; et al. Causes and Triggers of Deep-Seated Hillslope Instability in the Tropics—Insights from a 60-Year Record of Ikoma Landslide (DR Congo). *Geomorphology* **2019**, *345*, 106835. [[CrossRef](#)]
93. Francis, O.; Fan, X.; Hales, T.; Hobley, D.; Xu, Q.; Huang, R. The Fate of Sediment After a Large Earthquake. *J. Geophys. Res. Earth Surf.* **2022**, *127*, e2021JF006352. [[CrossRef](#)]
94. Wang, R.; Zhang, S.; Pu, L.; Yang, J.; Yang, C.; Chen, J. Gully Erosion Mapping and Monitoring at Multiple Scales Based on Multi-Source Remote Sensing Data of the Sancha River Catchment, Northeast China. *ISPRS Int. J. Geo-Inf.* **2016**, *5*, 200. [[CrossRef](#)]
95. Soms, J. Regularities of Gully Erosion Network Development and Spatial Distribution in South-Eastern Latvia. *Baltica* **2006**, *19*, 72–79.
96. Li, H.; Cruse, R.M.; Liu, X.; Zhang, X. Effects of Topography and Land Use Change on Gully Development in Typical Mollisol Region of Northeast China. *Chin. Geogr. Sci.* **2016**, *26*, 779–788. [[CrossRef](#)]
97. Yibeltala, M.; Tsunekawac, A.; Haregeweynd, N.; Adgoe, E.; Meshesha, D.T.; Aklogf, D. Analysis of Long-Term Gully Dynamics in Different Agro-Ecology Settings. *Catena* **2020**, *179*, 160–174. [[CrossRef](#)]
98. Kropáče, K.J.; Schillaci, C.; Salvini, R.; Marker, M. Assessment of Gully Erosion in the Upper Awash, Central Ethiopian Highlands Based on a Comparison of Archived Aerial Photographs and Very High Resolution Satellite Images. *Geogr. Fis. Dinam. Quat.* **2016**, *39*, 161–170. [[CrossRef](#)]
99. Radoane, M.; Ichim, I.; Radoane, N. Gully Distribution and Development in Moldavia, Romania. *Catena* **1995**, *24*, 127–146. [[CrossRef](#)]
100. Golosov, V.; Yermolaev, O.; Rysin, I.; Vanmaercke, M.; Medvedeva, R.; Zaytseva, M. Mapping and Spatial-Temporal Assessment of Gully Density in the Middle Volga Region, Russia. *Earth Surf. Process. Landf.* **2018**, *43*, 2818–2834. [[CrossRef](#)]
101. Medvedeva, R.A.; Golosov, V.N.; Ermolaev, O.P. Spatio-Temporal Assessment of Gully Erosion in the Zone of Intensive Agriculture in the European Part of Russia. *Geogr. Nat. Resour.* **2018**, *39*, 204–211. [[CrossRef](#)]